HREC-1347-5
LMSC/HREC D162128

LOCKHEED MISSILES & SPACE COMPANY

HUNTSVILLE RESEARCH & ENGINEERING CENTER

HUNTSVILLE RESEARCH PARK

4800 BRADFORD BLVD., HUNTSVILLE, ALABAMA

CR-102600

STUDY OF THERMAL CONDUCTIVITY REQUIREMENTS – HIGH PERFORMANCE INSULATION

FINAL REPORT

February 1970

Contract NAS8-21347

by

D. V. Hale

M. J. O'Neill

APPROVED BY: J. K. Lovin

J. K. Lovin, Supervisor
Thermal Environment Section

George D. Reny

G. D. Reny, Manager
Aeromechanics Dept.

for G. D. Reny

J. S. Farrior
Resident Director

FOREWORD

This report represents the results of work performed by the Thermal Environment Section of the Aeromechanics Department of Lockheed Missiles & Space Company, Huntsville Research & Engineering Center, for the National Aeronautics and Space Administration, Marshall Space Flight Center, Huntsville, Alabama, under Contract NAS8-21347. The NASA contract monitor was Mr. John Austin of the MSFC Astronautics Laboratory.

Also published under this contract, in fulfillment of Modification 4, is the following report:

"Preliminary Design of a High-Temperature Space Manufacturing Furnace," by V. Wayne Sparks, LMSC/HREC D162015, January 1970.

SUMMARY

Using Lockheed/Huntsville's electrical cylindrical calorimeter, an experimental study was performed to determine if high-temperature baking of mylar/polyurethane foam insulation composite could lower thermal conductivity of this high performance insulation specimen by expelling unwanted gases which had been absorbed, adsorbed, or chemisorbed within the composite. The results of this study showed that the conductivity cannot be reduced below the optimum value attainable by extended room-temperature outgassing. However, the amount of time necessary to totally outgas the composite is substantially reduced when such outgassing is accomplished at elevated temperatures, rather than at room temperature.

After the composite had reached the totally outgassed, optimum conductivity state, the specimen was exposed to the atmosphere for different periods of time to determine what thermal degradation would be caused by such exposure. Even after atmospheric exposure for more than three weeks, when the specimen was reinstalled in the vacuum chamber and the room-temperature conductivity measured, no degradation was found to have taken place. Therefore, once mylar/foam composite is totally outgassed, even long-term atmospheric exposure does not result in a return to the pre-outgas, high conductivity state.

An experimental study was also conducted for three different insulation systems which had as a spacer material polyurethane foam with slot cutouts in the foam, such that 50% of the foam was removed. The best of these cutouts had a conductivity as low as conventional mylar/foam composite and a density of about one-half the density of the conventional composite.

Standard thermal conductivity testing was conducted for four other high performance insulation composites, yielding conductivity as a function of temperature over a range of temperatures of -100° to 200°F, and room-temperature conductivity as a function of pressure over a range of pressures of 8×10^{-6} torr to one atmosphere. The composites tested were:

- Embossed mylar/Tissuglas at 62 layers per inch.
- Embossed mylar/nylon net at 50 layers per inch.
- Shallow dimpled Dimplar at 44 layers per inch.
- Embossed mylar/silk net at 56 layers per inch.

An insulation system was designed and fabricated for a 20-inch diameter subscale cryogen storage tank which will be tested by NASA-Marshall Space Flight Center. A computer thermal analysis was performed for the insulated tank. The high performance insulation system used was smooth mylar/nylon net, 1/4-inch in thickness, at a layer density of 80 layers per inch. The testing will yield valuable data on the conductivity of the composite in an actual application.

A comparison was made between thermal conductivity data obtained with the cylindrical calorimeter, and thermal conductivity predictions based on semi-empirical correlations developed by other investigators of high performance insulation. The data corresponded closely to the semi-empirical predictions, again verifying the accuracy of the calorimeter.

CONTENTS

CONTENTS (Continued)

LIST OF TABLES

LIST OF TABLES (Continued)

LIST OF ILLUSTRATIONS

LIST OF ILLUSTRATIONS (Continued)

LIST OF ILLUSTRATIONS (Continued)

NOMENCLATURE

A_c	calorimeter tube cross section
C_p	specific heat
d	error in a quantity
I	test section current
k	thermal conductivity
L	calorimeter test section length
m	mass
P	test section power
q	heat flux through insulation on test section
q_ℓ	longitudinal heat flow from test section
q_s	heat stored in test section
r	insulation specimen radius
t	calorimeter tube thickness
T	temperature
ΔT	$(T_i - T_o)$
V	test section voltage

Greek

θ	time
ρ	insulation density

NOMENCLATURE (Continued)

Subscripts

i	inside of insulation
ins	insulation
o	outside of insulation
1	glass fiber tube
2	copper heater wires

Section 1
INTRODUCTION

With the preliminary studies now underway for such bold space missions as the Space Station, the Mars Flyby, and the Grand Tour, the need for long term storage of cryogenic fluids, slushes, and solids in space environment has become increasingly apparent. To meet this need for long-term storage of cryogens for fuel and life support use, numerous high performance insulation (HPI) composites have been developed. With their development comes the need for accurate thermal conductivity data on each insulation composite.

In the past, HPI thermal conductivity data were most frequently obtained by using flat-plate or guarded-tank calorimeters, both of which impose a large temperature differential across the insulation specimen and measure the apparent thermal conductivity for the two boundary temperatures. The inherent disadvantage in both of these calorimeters is their inability to provide temperature-dependent thermal conductivity data for a wide range of temperatures.

In 1967, Lockheed/Huntsville developed a new thermal conductivity measurement apparatus designed to yield accurate temperature-dependent data for HPI composites. The apparatus is the electrical cylindrical calorimeter described in Section 2. This new calorimeter can operate with a small temperature differential across the insulation specimen, and with a wide range of mean temperatures, thus allowing thermal conductivity to be accurately measured as a function of temperature. The cylindrical calorimeter operates with a temperature differential of about $40^{\circ}F$, while flat plate calorimeters operate with a temperature differential of about $400^{\circ}F$. The calorimeter uses a central test heater, two longitudinal guard heaters, and two end guard heaters. The two longitudinal heaters are operated at the same power density level as the test heater, thereby preventing a power density change at the ends of the test heater. The end heaters are operated at a higher power density level

to compensate for heat losses out the ends of the calorimeter and to maintain the temperature of the longitudinal heaters at the same level as that of the test heater. With a constant power density level and temperature across the ends of the test heater, this test section closely approximates a section of an infinite cylinder. Using the solution of the heat conduction equation for an infinite cylinder, precise thermal conductivity data can be obtained with this calorimeter.

Since the calorimeter was first developed, many refinements have been made, in design and test operation, which have increased accuracy and minimized cost of acquiring data. Calorimeter design, operation, and accuracy are discussed in Section 2.

The cylindrical calorimeter was used in three testing tasks of this study: (1) bake and degas; (2) foam cutout; and (3) standard thermal conductivity. Results of these tasks are discussed in Sections 3, 4 and 5, respectively.

In addition to the cylindrical calorimeter tests that were performed, a thermal insulation system for a subscale cryogen storage tank was designed, fabricated and computer-analyzed under this contract. The system will be tested at NASA/MSFC.

The data obtained from analysis and by testing the insulation system in an actual prototype application yields another measure of the thermal performance of the composite tested. The tank test and analysis are described in Section 6.

Information obtained during this study is presented as follows:

Section 2 Calorimeter Design, Operation and Accuracy

Section 3 Bake and Degas Testing (Task I)

Section 4 Foam Cutout Testing (Task II)

Section 5 Standard Thermal Conductivity Testing (Task III)

Section 6 Subscale Tank Insulation System Analysis and Testing (Task IV)

Section 7 High Performance Insulation Conductivity Data Comparison.

Each section of this report presents all the information pertaining to that subject that was obtained during this study, except references, tables, and figures, which are found on pages 27 through 67.

Section 2
CALORIMETER DESIGN, OPERATION, AND ACCURACY

2.1 CALORIMETER DESIGN AND SPECIMEN APPLICATION

Lockheed/Huntsville's electrical cylindrical calorimeter, shown in the photograph in Fig. 1 and schematically in Fig. 2, consists of a 38-in. long, 3 in.-outside diameter, 1/16-in. thick silicone glass fiber tube, onto which is wound 6-mil copper magnet wire to form five heaters. There are no gaps between adjacent windings, nor are there gaps between heaters. The result is that 38 in. of uniform, continuous windings completely cover the base cylinder. The 1-ft. long test heater is located at the longitudinal center of the calorimeter and is flanked by two 1-ft. long "longitudinal" heaters. On each end, adjacent to the longitudinal heaters, is located a 1-in. long end heater. Two 3-mil copper/constantan differential thermocouples connect the center of each longitudinal heater to the center of the test heater. Two other differential thermocouples of the same materials connect the center of each end heater to the center of the adjacent longitudinal heater. These four thermocouples monitor the longitudinal temperature gradient along the calorimeter. Another thermocouple, located at the center of the test heater, monitors the absolute temperature there, by reference to an LN_2 bath.

The entire calorimeter is wrapped with a specimen of the HPI composite to be tested. The longitudinal portion of the calorimeter is wrapped circumferentially in either of two ways: (1) by separate sheets of the composite cut and applied for each layer, or (2) by a long, continuous strip of the composite rolled onto the calorimeter. The second method is quicker and more economical, and was used for most of the specimens wrapped under this study. The ends of the calorimeter are covered with circular pieces of insulation,

which meet the longitudinal portion of the specimen at a 45-deg diagonal joint, as shown in Fig. 3. Instrumentation wires and support cords exit the insulation at these joints.

Inside a vacuum chamber, the wrapped calorimeter is installed in an environmental control shroud, which maintains the outside of the insulation specimen at a desired, uniform temperature. By supplying power to the calorimeter heaters, a slightly higher temperature is maintained inside the insulation specimen than outside. The temperature differential from the inside of the insulation to the outside is measured by a differential thermocouple. The known power, temperature differential, insulation thickness, and test section length establish the thermal conductivity of the composite after steady state conditions have been achieved.

2.2 CALORIMETER OPERATION

After the calorimeter has been wrapped with the insulation to be tested and installed inside the shroud in the vacuum chamber, the chamber is evacuated to a pressure of $\leq 8 \times 10^{-6}$ torr. The calorimeter is then heated or cooled to the desired temperature either by heating the shroud with hot compressed air, or by cooling the shroud with liquid nitrogen. When the calorimeter attains the desired temperature, the inside is heated to a slightly higher temperature than the outside by supplying power to the calorimeter heaters. When the desired temperature drop across the insulation is obtained, a fixed power is set into the test and longitudinal heaters to maintain the temperature at a constant level. The end heaters are automated to maintain a slightly higher temperature than the longitudinal heaters to compensate for heat loss out the instrumentation wiring of the calorimeter. Before steady state conditions are achieved, the test heater temperature is monitored and adjustments made in test and longitudinal heater power to keep the temperature constant. If the temperature of the longitudinal heaters rises above or falls below the temperature of the test heater, the power to the end heaters is reduced or increased, respectively.

When the temperature is constant with time and the temperature is the same at the center of the test heater as it is at the center of each longitudinal heater, steady state has been achieved.

When steady state is reached, the power and temperature distributions along the calorimeter assume the shapes shown in Fig. 4. With such distributions, the test section of the calorimeter, between the dashed lines in the figure, very accurately approximates a section of an infinite cylinder. Therefore, the solution to the heat conduction equation for an infinite cylinder can be applied to arrive at the effective thermal conductivity of the composite. The pressure inside the calorimeter is measured with an ion pressure gauge before going to a new data point.

2.3 CALORIMETER ACCURACY

The following error analysis gives a reasonable indication of the calorimeter accuracy. The specimen considered is double-aluminized mylar and red polyurethane foam.

The equation required to determine the thermal conductivity is

$$k(T) = \frac{q \ln \left(\frac{r_o}{r_i}\right)}{2\pi L(T_i - T_o)}$$

where

$$T = \frac{T_o + T_i}{2}$$

$$q = P = IV$$

In order to determine the error in k(T), the errors in q, r_o, r_i, L and $T_i - T_o$ must be determined and combined. The Kline-McClintock probable error analysis procedure shown in Appendix A is used to obtain the combined effect of the errors on k. The best estimate for the probable error for each parameter is determined below:

$r_i = \frac{1.5}{12}$ ft $\qquad dr_i = \frac{0.02}{12}$ ft

$r_o = \frac{2.5}{12}$ ft ($\frac{2.0}{12}$ for embossed aluminized Mylar) $\qquad dr_o = \frac{0.1}{12}$ ft

$$d\left(\frac{r_o}{r_i}\right) = \left\{\left(\frac{dr_o}{r_i}\right)^2 + \left(\frac{r_o\, dr_i}{r_i^2}\right)^2\right\}^{1/2}$$

$$= \left\{\left(\frac{0.1/12}{1.5/12}\right)^2 + \left[\frac{(2.5/12)\,(0.02/12)}{(1.5/12)^2}\right]^2\right\}^{1/2}$$

$$= 0.0703$$

$$d\left(\ln \frac{r_o}{r_i}\right) = \frac{1}{\left(\frac{r_o}{r_i}\right)} \cdot d\left(\frac{r_o}{r_i}\right)$$

$$= \frac{0.0703}{\left(\frac{2.5/12}{1.5/12}\right)} = 0.0422$$

$$\frac{d\,\ln\left(\frac{r_o}{r_i}\right)}{\ln\left(\frac{r_o}{r_i}\right)} = \frac{0.0422}{0.51} = 8.3\%$$

$L = 1$ ft $\qquad dL = \frac{0.05}{12}$ ft

$$\therefore \quad \frac{dL}{L} = \frac{0.05/12}{1} = 0.00417 = 0.417\% \text{ (negligible)}$$

$$(T_i - T_o) \approx 40^\circ R \qquad d(T_i - T_o) = 0.05^\circ R$$

$$\frac{d(T_i - T_o)}{(T_i - T_o)} = \frac{0.05}{40} = .00125 = 0.125\% \text{ (negligible)}$$

$$q = P = IV \qquad dq = d(IV) \pm q_\ell \pm q_s$$

$$d(IV) = 0.0014\ IV$$

$$\frac{d\,IV}{IV} = 0.0014 = .14\% \text{ (negligible)}$$

The longitudinal heat loss, q_ℓ, is calculated using conduction in the glass fiber and in the insulation. Conduction down the copper wire is small in comparison to that in the glass fiber and insulation. The largest temperature difference between the test and a longitudinal heater is $1/20^\circ F$.

$$q_\ell = k_c A_c \frac{\Delta T}{\Delta X} + \frac{1}{2} k_{ins} A_{ins} \frac{\Delta T}{\Delta X}$$

The 1/2 precedes the insulation term because the temperature gradient $\frac{\Delta T}{\Delta X}$ exists for the inner boundary of the insulation, while the outer boundary is at a constant temperature. The average $\frac{\Delta T}{\Delta X}$ therefore is $\frac{1}{2}\ \frac{\Delta T}{\Delta X}$.

Using the following known values,

$k_c = 0.182$ Btu/hr-ft-$^\circ$F $\quad k_{ins} = .024$ Btu/hr-ft-$^\circ$F (24 layers of DAM)

$A_c = 2\pi r_i t \quad A_{ins} = \pi(r_o^2 - r_i^2) = \frac{\pi(2.5^2 - 1.5^2)}{144} = .0872$ ft^2

$= \frac{2\pi\, 1.5(1/16)}{144}$ ft^2 $= .00408$ ft^2

$$\frac{\Delta T}{\Delta X} = \frac{1/20^\circ F}{1 \text{ ft}} = 0.05$$

$$q_\ell = 0.000372 \text{ Btu/hr} + .0001045 \text{ Btu/hr for one end}$$

$$\therefore q_\ell = \left[2\left[.0004765\right]^2\right]^{1/2} = 0.00068 \text{ Btu/hr} \left\{ \begin{array}{l} \text{Probable error} \\ \text{for both ends} \end{array} \right.$$

The heat stored term q_s is calculated from the thermal mass of the test section of the calorimeter. During operation the largest temperature change with time of the calorimeter was 0.02°F/hr

$$q_s = \left(m_1 C_{p_1} + m_2 C_{p_2}\right) \frac{\Delta T}{\Delta \theta}$$

where

$m_1 = 0.464$ lb$_m$

$C_{p_1} = 0.27$ Btu/lb$_m$-$^\circ$F

$m_2 = 0.16$ lb$_m$

$C_{p_2} = 0.1$ Btu/lb$_m$-$^\circ$F

$\frac{\Delta T}{\Delta \theta} = 0.02\ ^\circ$F/hr

$$q_s = \left[(0.464)(0.27) + (0.16)(0.1)\right] 0.02$$

$$= 0.00282 \text{ Btu/hr}$$

Now the combined probable error of q_ℓ and q_s is calculated

$$dq = (0.00068^2 + .00282^2)^{1/2}$$

$$= 0.00291 \text{ Btu/hr}$$

For a room temperature point with this specimen, q = .0452 Btu/hr

$$\frac{dq}{q} = \frac{.00291}{.0452}$$

$$\therefore \quad \frac{dq}{q} = 0.0644 = 6.44\%$$

Now all the errors are combined to obtain the error in thermal conductivity. The Kline-McClintock rms method of combining errors is used. All the above errors except $d\,\ell n\,(r_o/r_i)\,/\,\ell n\,(r_o/r_i)$ and dq/q are insignificant in an rms summation. Therefore,

$$\frac{dk}{k} = \left\{ \left[\frac{d\,\ell n \left(\frac{r_o}{r_i}\right)}{\ell n \left(\frac{r_o}{r_i}\right)} \right]^2 + \left[\frac{dq}{q}\right]^2 \right\}^{1/2}$$

$$= \left[8.3\%^2 + 6.44\%^2\right]^{1/2}$$

$$\therefore \frac{dk}{k} = 10.5\%$$

This error is typical of the error encountered at other low-conductivity data points. At higher temperatures and pressures, the error is reduced because the power supplied to the heaters is much larger, making $\frac{dq}{q}$ much smaller.

2.4 ENVIRONMENTAL CONTROL APPARATUS

Under a previous NASA contract, Lockheed/Huntsville constructed a vacuum chamber for conducting thermal conductivity tests on HPI systems. The chamber was designed specifically to meet the requirements of the thermal tests with the two primary criteria: (1) precise thermal control, and (2) speed of operation. This chamber is shown in Fig. 5. The nominal dimensions are 17.5 in. inside diameter and 52 in. long. The chamber was constructed by butting a stainless steel, right circular cylinder chamber 23 in. long, against a glass bell jar chamber 30 in. long. An aluminum shroud 14 in. inside diameter and approximately 47 in. long is used to provide a controllable thermal environment for the test specimen. A copper coil encloses the aluminum shroud, and the fluid is circulated through the coil for thermal control of the shroud. The shroud and coil are enclosed in an HPI blanket to minimize heat leakage between the shroud and the chamber.

The shroud can be either heated by hot air or cooled by liquid nitrogen. Heated air is supplied to the shroud coil through a thermostat-controlled electric gas heater, and is vented to the atmosphere. The temperature setting and flow rate can be adjusted to maintain the shroud at almost constant temperature ($\pm 2^{\circ}F$).

For the cooling mode, LN_2 is supplied by a 25-gal dewar situated near the vacuum chamber. A thermocouple in series with a variable reference voltage is used as input to an amplifier which controls a relay, which in turn actuates a valve in the LN_2 supply line. The thermocouple measures the temperature difference between an LN_2 bath and the environmental shroud. The reference voltage is set to match the emf that the thermocouple would produce when the shroud is at the temperature desired. The LN_2 is vented to the atmosphere after it passes through the shroud coil. By having a short supply line between the dewar and the shroud, the temperature variations of the shroud during operation are held to a minimum ($\leq 8^{\circ}F$). The HPI blanket around the shroud minimizes the number of LN_2 flow cycles. A typical cycle

is two to three hours. However, the oscillations in the shroud temperature are impressed on the outside of the specimen insulation requiring that the average ΔT across the specimen insulation be used in calculating a data point. The ΔT, therefore, must be much greater than the temperature variation of the shroud. A ΔT of $30^{\circ}F$ or greater is sufficient.

Section 3
TASK I: BAKE AND DEGAS TESTING

3.1 BAKE PRECONDITIONING OF MYLAR/FOAM COMPOSITE

Testing performed under Contracts NAS8-21134 and NAS8-21347 indicated that the thermal conductivity of mylar/foam composite decreased appreciably after being baked at elevated temperatures. In the present contract, an experimental study was conducted to determine whether such baking would be a valuable preconditioning method to be used prior to flight to achieve optimum thermal performance of the mylar/foam composite.

A specimen of mylar/foam composite, with a layer density of 23 layers per inch, was outgassed by rough pumping and diffusion pumping at full capacity at room temperature for nine days, and the room temperature conductivity continually decreased as the pressure decreased, until the conductivity leveled off at 8.45×10^{-5} Btu/hr-ft-^{o}F and the pressure at 3.4×10^{-6} torr. The specimen was then baked at 200^{o}F to determine if the conductivity would be improved by such preconditioning. The room temperature conductivity after baking for 16 days was 8.16×10^{-5} Btu/hr-ft-^{o}F. Thus, no appreciable improvement was caused by baking at 200^{o}F. Table 1 and Fig. 6 present these two data points.

Next, a 300^{o}F bake was attempted to see if a greater temperature might be required for effective preconditioning. During heatup to 300^{o}F, a pause was made at 250^{o}F to obtain a data point at that temperature. The point is shown in Table 2 and Fig. 6, and it fits well on the conductivity curve of mylar/foam composite, previously obtained with the cylindrical calorimeter. After this pause, the heatup to 300^{o}F was completed. Exposure to this temperature damaged the specimen physically and degraded it thermally, causing the foam to change in color, and the mylar to flake at hot spots. Excessive quantities of carbon dioxide were observed in the vacuum chamber by residual gas analysis at this time, and the test was discontinued. Apparently, oxidation of some

chemical constituents of the insulation and calorimeter caused carbon dioxide to form. The residual gas analyses are discussed below in greater detail.

Since both prolonged room temperature outgassing and 200°F baking resulted in essentially the same value of conductivity at room temperature ($8 - 8.5 \times 10^{-5}$ Btu/hr-ft-°F), it was concluded that either method could be used to obtain the totally outgassed, minimum conductivity state of the composite. However, bake preconditioning could still be of value if it considerably reduced the amount of time required to reach this optimum state. In order to determine if baking would indeed expedite greatly the outgassing process, a new specimen of mylar/foam composite, again at 23 layers per inch, was fabricated and baked for a period of 24 hours at a mean temperature of 230°F. After the bake, a room temperature conductivity measurement was made and, as shown in Table 3 and Fig. 6, the room temperature conductivity had reached the optimum state.

The conclusion from the data is that while the optimum conductivity state can be reached in about nine days by room temperature outgassing, the optimum state can be reached by a high temperature bake of relatively short duration ($\leq$ 24 hours). It must be noted, however, that four days elapsed during cool-down from the 230°F bake and during room temperature data point stabilization, perhaps contributing to the reduction in conductivity attributed to the bake.

3.2 RESIDUAL GAS ANALYSES OF SPECIES EXPELLED DURING BAKE TESTS

Using a Consolidated Electrodynamics Corporation 21-612 RGA analyzer, residual gas analyses were conducted at 250°F, 300°F, and during cool-down after 300°F. The gases present in large quantities were nitrogen (N_2), oxygen (O_2), water vapor (H_2O), carbon dioxide (CO_2), and hydrocarbon gases from the diffusion pump oil. In the table on the following page, the species of gases determined by each test are listed and their relative proportions are specified according to partial pressure.

RESIDUAL GAS ANALYSES OF OUTGASSING SPECIES

Gas Species	Pressure % of Each Gas at 250°F Data Point 11 July 1969	Pressure % of Each Gas at 300°F Data Point 22 July 1969	Pressure % of Each Gas During Cooldown After 300°F Data Point 24 July 1969
H_2O	12.2	14.8	18.3
N_2	69.7	39.9	64.0
O_2	16.4	14.0	15.8
CO_2	0.0	25.6	1.9
Pump Oil Hydrocarbons	1.7	5.7	0.0
Total	100.0	100.0	100.0

The nitrogen and oxygen were detected in amounts that are in the same ratio as the ratio of nitrogen and oxygen in air. Since most of the gas analyzed was composed of these two gases, it appears that the outgassing substance is mostly air. The percentage of water vapor in the gases was, however, much higher than the percentage of water vapor in normal air. The relatively large amount of water vapor present apparently was due to expulsion of water vapor molecules from the insulation and from the vacuum system. These molecules had been trapped by absorption, chemisorption, and/or adsorption by the insulation and vacuum system. The high temperature bake increased the thermal agitation and pressure of the molecules and facilitated their escape.

Carbon dioxide was found in small or negligible percentages in two of the tests, but at 300°F, carbon dioxide was present at 25.6% of the total pressure. This excessively high content of carbon dioxide shows that some components of the insulation and/or the system had oxidized. When the specimen was inspected after being tested, a nylon support cord had broken, the electrical wiring insulation had discolored, the polyurethane foam had shrunk and

discolored, and the mylar had melted in places, leaving loose flakes of aluminum which had previously been bonded to it. Combined oxidation of the insulation specimen and the components of the electrical and support systems apparently led to the excessively high percentage of carbon dioxide. Hydrocarbons from the diffusion pump oil, always present in vacuum systems of this type, were present in small quantities.

The conclusion to be drawn from the high content of water vapor found to be present in each of the analyses is that high-temperature baking does indeed liberate entrapped water vapor molecules from the insulation composite. However, as documented in Section 3.1, such degrading molecules can also be expelled by long-term room-temperature outgassing, although such a process takes longer than high-temperature outgassing.

3.3 ATMOSPHERIC DEGRADATION TESTING

The purpose of the degradation series of tests was to determine the effect of atmospheric exposure upon thermal conductivity of mylar/foam composite. Starting with a totally outgassed specimen, the specimen was exposed to the atmosphere for different lengths of time to determine if such exposure would degrade the composite to its original, unoutgassed, high-conductivity state. Starting with the mylar/foam specimen which had been outgassed at 230°F for 24 hours, and which had reached the optimum room-temperature conductivity, the specimen was exposed to the atmosphere for durations of 3 minutes, 70 minutes, 25 hours, and 24 days, each exposure period being followed by a room-temperature conductivity data point. Somewhat surprisingly, the conductivity after each exposure period was still at the optimum value, as shown in Table 3 and Fig. 7.

The conclusion from these test data is that once mylar/foam composite is sufficiently outgassed, atmospheric exposure, even of long duration, does not cause the composite to degrade to its original, unoutgassed condition. It could prove valuable, therefore, to outgas thoroughly mylar/foam insulation composite prior to its use in a flight application. This could most easily be done before the composite is fabricated into an insulation system.

Section 4
TASK II: FOAM CUTOUT TESTING

4.1 EMBOSSED MYLAR/CUTOUT FOAM SPECIMEN TESTING

Theoretically, mylar/foam composite could be substantially improved in both thermal conductivity and weight density by removing portions of the foam. The removed foam would decrease solid conduction and also cause the mylar to become favorably non-isothermal, both effects yielding a decrease in apparent thermal conductivity. This decrease in theoretical conductivity was indicated by computer thermal analysis. The density improvement is obvious, the density being reduced in direct proportion to the amount of foam removed.

To test the theory, a specimen of embossed mylar/cutout foam was fabricated with 50% of the foam removed by slot cutouts in the foam layers, as depicted schematically in Fig. 8. The alternate layers of cutout foam had the cutouts rotated 90 deg in orientation. The sheets were placed on the calorimeter in random fashion with no attempt to align the slots in one sheet with those in any other sheet, since this configuration would have good thermal and structural properties, and would be easily fabricated.

Although thermal shorting through the holes in the foam was expected between mylar sheets above and below the holes, the extent of shorting was not analytically determinable. Thermal testing revealed that apparently a great amount of shorting occurred, even though embossed mylar had been used to reduce contact area between shorting sheets. As evident from Fig. 9 and Table 4, the thermal conductivity was increased, rather than decreased, by the removal of the foam.

Other causes of the higher conductivity for the cutout composite should also be noted. First, embossed mylar is substantially thicker than smooth mylar and therefore lays up at a lower layer density, when approximately the same fabrication compression is applied. The cutout composite had a layer density of 20 layers per inch, compared to 23 for regular mylar/foam specimens. This accounted for more radiation through the insulation, thereby increasing apparent conductivity. Secondly, since the actual compressive load was not measured in either composite, it is quite possible that the compressive load was significantly higher in the cutout composite, due to the much greater thickness of the embossed mylar, which would decrease contact resistance and elevate conductivity.

To prevent thermal shorting, Tissuglas spacers were placed between the mylar and cutout foam in the second cutout specimen. When this cutout foam/Tissuglas/embossed mylar specimen was tested even more interesting data were obtained. Although thermal shorting had been prevented, the thermal conductivity increased again, even above the first cutout tested, as shown in Table 4 and Fig. 9.

This apparent paradox can also be logically explained. With the added thickness of the Tissuglas, the composite was laid up at 19 layers per inch, as opposed to 20 for the first cutout, and 23 for the regular mylar/foam composite. This decrease in layer density increased radiation through the insulation. Far more important, however, is the fact that the 19 sheets of Tissuglas, which were added to the composite, were effectively squeezed between the mylar and foam layers, increasing considerably the compressive load between layers. This increased compression lowered contact resistance between layers and increased thermal conductivity so greatly that the reduction in thermal shorting was not noticeable.

From the data, it was concluded that compressibility effects had caused the first two cutout designs to have poor thermal conductivities. Therefore,

a third cutout specimen was designed to reduce compression, as discussed in the next sub-section of this report.

The results of these first two cutout tests emphasize the great effect of compressive load and layer density upon thermal conductivity of HPI composites. For a more detailed examination of these effects on several types of HPI systems see Ref. 1, an Interim Report published under this contract.

4.2 SMOOTH MYLAR/CUTOUT FOAM/TISSUGLAS SPECIMEN TESTING

To improve the performance of the next cutout foam insulation composite, compressibility effects were considered in the third cutout specimen design. Three design constraints were imposed: (1) minimal thermal shorting; (2) high layer density; (3) low compressive load. To meet these constraints, smooth mylar – because it is thinner – was used in place of the thicker embossed mylar. This thinner radiation shield allowed fabrication at a layer density of 20 rather than 19 (for the previous cutout composite), and the compressive load was substantially reduced.

As expected, the conductivity was greatly improved, as shown in Tables 4 and 5 and Fig. 9. The conductivity is as low as the optimum conductivity of regular mylar/foam composite. A perhaps more valuable comparison of this final cutout's thermal performance is presented in Fig. 10, together with data for the first cutout and for regular mylar/foam composite. The parameter, ρK, is valuable in comparing candidates for the weight-limited insulation system. As apparent in Fig. 10, this smooth mylar/cutout foam/Tissuglas composite has a ρK value slightly more than one-half the value for conventional mylar/foam composite at room temperature.

The improved performance of this third cutout composite was due to compressibility considerations in its design. More thorough experimental studies in the area of compressibility effects are strongly recommended.

Section 5
TASK III: STANDARD THERMAL CONDUCTIVITY TESTING

Standard thermal conductivity testing involved the experimental determination of thermal conductivity as a function of temperature, and room temperature conductivity as a function of chamber pressure, for four different HPI composites. The following composites were tested:

1. Embossed mylar/Tissuglas at 62 layers per inch
2. Embossed mylar/nylon net at 50 layers per inch
3. 1/2-mil shallow dimpled Dimplar at 44 layers per inch
4. Embossed mylar/silk net at 56 layers per inch

Results of these tests are presented in tabular form and graphical form in Tables 6 through 13 and Figs. 11 through 18, respectively.

The curves are typical HPI conductivity curves, except for the nylon net/embossed mylar composite. Because it is widely known that nylon net outgasses excessively (formaldehyde, a sizing agent, generally being one outgassing species), a room temperature data point was obtained after outgassing at 200°F, as shown in Fig. 13. It falls well below the unoutgassed conductivity curve, indicating the large effect of outgassing on thermal conductivity for this composite. This effect is discussed later in Section 6, since nylon net was selected as the spacer material for the subscale tank insulation system test documented in that section.

Section 6
TASK IV: SUBSCALE TANK TESTING AND ANALYSIS

6.1 INSULATION SYSTEM DESIGN

To determine the thermal conductivity of an HPI composite in an actual flight application, with its related variations in insulation compression, thickness, and temperature, subscale cryogen storage tank insulation system tests are conducted at NASA/MSFC. Under this study, Lockheed/Huntsville designed and fabricated an insulation system for a 20-in. diameter subscale test tank belonging to NASA, which will be tested at MSFC.

Of the six HPI composites examined in Ref. 1, the mylar/nylon net composite has the best thermal response to compressive load variation. Because of the low conductivity, the low density-conductivity product, and the low sensitivity to compressive load for nylon net composite, this insulation material was selected for use on the subscale tank insulation system. Fig. 19 presents data for the conductivity of this composite (at the boundary temperatures which will be used during this test) as a function of layer density. These data were documented in Ref. 2, a Lockheed/Sunnyvale report. From this figure, it is evident that the layer density corresponding to minimum conductivity is between 80 to 100 layers per inch. Therefore, the composite was applied to the subscale tank at a density of approximately 80 layers per inch.

In Section 5, it was pointed out that nylon net has a tendency to outgas, thereby degrading thermal performance. In order to prevent this undesirable phenomenon from occurring during the tank test, the nylon net was thoroughly baked and outgassed for two days in a vacuum chamber at Lockheed/Huntsville before it was fabricated for use in an insulation system. The bake temperature was 150°F, the duration was 48 hours, and the chamber pressure fell below 1×10^{-4} torr. This preconditioning should eliminate outgassing as a problem during the testing.

The basic purpose of the subscale tank testing is to determine the thermal conductivity of the insulation composite applied on the tank. However, as discussed in Ref. 3, for a tank as small as the 20-in. diameter tank, the heat leak to the cryogenic liquid down the tank neck (penetration) is the same order of magnitude as the heat leak through the HPI when an inch or more of HPI is used on the tank. Therefore, in order to keep the heat leak through the HPI considerably larger than the penetration heat leak, only 1/4 in. of HPI was applied to the tank. This should allow a better measurement to be made of conductivity, since the penetration heat leak will be only a small percentage of the HPI heat leak.

Two other measures were taken in designing the insulation system to eliminate the penetration heat leak as an error-causing parameter. A cooling coil was installed at the top of the tank neck, as shown in Fig. 20, through which liquid nitrogen will flow during some tests. This will reduce the penetration heat leak by cooling the penetration. The other means of reducing the heak leak down the penetration was the installation of a calibrated electric resistance heater inside the tank to allow control of the boiloff rate during the tests. By supplying power to the heater, the boiloff rate can be increased, thus causing more convective cooling of the neck of the tank. This cooling of the neck reduces the penetration heat leak. The true heat leak through the HPI can be obtained by subtracting the power supplied by the heater from the total heat absorbed by the cryogen during vaporization.

Several tests will be run with and without neck cooling, and with different powers to the heater. Valuable data should be obtained on the conductivity of mylar/nylon net composite in an actual prototype application. Also, data will be obtained on the penetration heat leak and its functional dependency upon flow rate and neck cooling.

6.2 INSULATION SYSTEM FABRICATION

A schematic of the tank is shown in Fig. 21. The cylindrical surface can be easily wrapped with HPI, but the ellipsoidal ends are more difficult

to wrap because of their three-dimensional curvature. A method was developed, however, that allowed the ends and cylinder of the tank to be wrapped with one piece of insulation.

To avoid gaps in the insulation, the cylindrical and elipsoidal surfaces of the tank were wrapped simultaneously with one piece of insulation. To allow a smooth, uniform layering on the ellipsoidal surfaces, this single piece of insulation was pre-cut to accurately fit the ellipsoidal ends. This was accomplished by pre-cutting 16 ellipsoidal lunes to fit each end. The lunes converge at the apexes of the ellipsoids and are small enough to approximate an ellipsoidal surface. The nylon lunes butt together, while the mylar lunes are allowed a small overlap for greater gap prevention. Another piece of insulation was used for the neck, and it was applied at the same time as the tank insulation layer, using overlap for the mylar junction and butting for the nylon junction.

Figures 22 through 26 show the tank during different stages of the wrapping operation. Twenty layers each of 1/4-mil double aluminized mylar and 9-mil nylon net were applied with a thickness of 1/4-in. to establish a layer density of 80 layers per inch, an optimum density for thermal conductivity.

Six 5-mil copper/constantan thermocouples were placed at the locations shown in Fig. 27. These thermocouples monitor the temperature gradient down the neck and through the insulation.

The cooling coil was made of 5/8-in. o.d. copper tubing and was wrapped six times around the tank neck and soldered in place. Aluminum foil beneath the coil allows a good heat conduction path and lowers contact resistance between the coil and neck.

The electric resistance heater will be installed inside the tank by NASA/MSFC before testing and will be used to control flow rate.

6.3 COMPUTER THERMAL ANALYSIS

A computer thermal analysis was conducted for the tank and insulation system to determine what should occur during the different phases of the testing. Eight cases were considered — five cases with different flow rates with the HPI conductivity input as a function of temperature (using a semi-empirical correlation presented in Ref. 2 to relate conductivity to temperature), and three cases with eqilibrium flow rates for three different effective HPI conductivities. In Fig. 28, the total heat leak to the liquid as a function of flow rate is presented. The dashed horizontal line is the heat leak due to the heat flow through the HPI below the liquid level, which is independent of flow rate. From Fig. 28, it is evident that the total heat leak is reduced with higher flow rates. This is due to the convective cooling of the neck, which reduces the penetration heat leak to the cryogen. At an infinite flow rate, the total heat leak to the liquid is only slightly greater than the heat leak through the HPI below the liquid level, because the penetration heat leak has been minimized. When the test data are reduced, showing the effect of flow rate on total heat leak, a curve of the heat leak versus flow rate should resemble the analytical curve in Fig. 28, providing that the assumed conductivity is a reasonably accurate estimate.

The straight line beginning at the origin represents the heat required to maintain the flow rate, or $h_v \dot{m}$, and the point where this curve intersects the total heat leak curve is the equilibrium flow rate, or boiloff rate.

In Fig. 29, the total heat leak to the cryogen is shown as a function of the HPI effective conductivity. The conductivity value of 2×10^{-5} Btu/hr-ft-^{o}F corresponds closely to the effective conductivity (as an integrated average of the temperature-dependent data) used in the first five cases. If the assumed conductivity used in the first five cases was low or high, the measured heat leak during the test will be larger or smaller than that predicted in Fig. 28. If the value of effective conductivity should have been input as

either 0.5×10^{-5} or 5.0×10^{-5} Btu/hr-ft-^{o}F, the total heat leak at equilibrium should correspond to one of those two points in Fig. 29. The dashed line in Fig. 29 is the heat leak through the HPI below the liquid level, which is very nearly a linear function of HPI conductivity.

These curves can be compared later to the experimental data obtained by NASA/MSFC.

6.4 TESTING OF THE INSULATED TANK

The insulated tank will be delivered to NASA/MSFC in February 1970 with a detailed test plan. NASA/MSFC personnel are conducting the tests, and will reduce the data. Since the tests were not conducted during the contract, a comparison of theoretical and experimental results cannot be made.

Section 7
HIGH PERFORMANCE INSULATION CONDUCTIVITY DATA COMPARISON

HPI investigators have developed semi-empirical relations relating thermal conductivity to boundary temperatures, layer density, and emissivity. In Figs. 30 through 33, a graphical comparison is presented between Lockheed/Huntsville's cylindrical calorimeter data and the semi-empirical correlations which should describe the conductivity, when the proper independent variables are used in the equations.

The comparison shows that the experimental data compare quite well with the predicted conductivity from the semi-empirical correlations. For a more detailed comparison, see Ref. 1. This comparison between experimental and semi-empirical conductivities again verified the accuracy of the cylindrical calorimeter.

REFERENCES

1. Hale, D. V., and M. J. O'Neill, "High Performance Insulation Compressibility Study," LMSC/HREC D149187, Lockheed Missiles & Space Company, Huntsville, Ala., November 1969.

2. Lockheed Missiles & Space Company, "Investigations Regarding Development of a High Performance Insulation System," LMSC-K-17-68-5, Sunnyvale, Calif., 25 July 1968.

3. Hale, D. V., "MSFC 20-Inch and 105-Inch Cryogenic Tank Analyses," LMSC/HREC D148760, Lockheed Missiles & Space Company, Huntsville, Ala., June 1969.

TABLES

Table 1

EFFECT OF DURATION OF 200°F BAKE ON 100°F THERMAL CONDUCTIVITY AFTER PREVIOUS EXTENDED ROOM TEMPERATURE OUTGASSING

Mean Insulation Temp. (°F)	ΔT °F	Duration of Room Temp. Outgassing (days)	Duration of 200°F Bake (days)	Chamber Pressure (torr)	Insulation Backside Pressure (torr)	Thermal Conduct. ($\times 10^5$) (Btu/hr-ft-°F)
104.3	43.2	9	0	3.4×10^{-6}	4.2×10^{-4}	8.45
101.35	40.7	9	16	1.7×10^{-7}	1.6 to 2×10^{-5}	8.16

Table 2

THERMAL CONDUCTIVITY OF DOUBLE-ALUMINIZED MYLAR/ POLYURETHANE FOAM SPECIMEN AT 250°F

Mean Insulation Temperature (°F)	ΔT (°F)	Internal Pressure (torr)	Thermal Conductivity (Btu/hr-ft-°F)
254.35	28.1	2×10^{-4}	40.3×10^{-5}

Table 3

ROOM-TEMPERATURE DATA POINTS TAKEN AFTER ATMOSPHERIC EXPOSURE FOR BAKE AND DEGRADATION SPECIMEN

Duration of Atmospheric Exposure	Mean Insulation Temperature (^{o}F)	ΔT (^{o}F)	Chamber Pressure (torr)	Thermal Conductivity (Btu/hr-ft-^{o}F x 10^{5})
None	116.25	67.1	10×10^{-6}	9.75×10^{-5}*
3 min	121.85	76.1	9.4×10^{-6}	10.82
70 min	121.1	76.2	1.3×10^{-5}	11.0
25 hr	102.8	41.0	10×10^{-6}	8.12
24 days	99.05**	38.9	1.2×10^{-5}	8.16**

* After 24 hours of 230^{o}F outgassing

** The differences in conductivity are due to differences in temperature and are not due to different degrees of outgassing.

Table 4

DATA POINTS FOR THE THREE CUTOUT COMPOSITES

Composite Number	Mean Insulation Temperature (^{o}F)	ΔT (^{o}F)	Chamber Pressure (torr)	Internal Pressure (torr)	Thermal Conductivity (Btu/hr-ft-^{o}F)
1	103.8	33.4	1.3×10^{-5}	—	17.7×10^{-5}
1	-51.5	265.7	7.0×10^{-6}	—	7.94×10^{-5}
2	108.4	38.2	1.7×10^{-5}	4.1×10^{-4}	21.2×10^{-5}
2	-47.9	245.8	9.2×10^{-6}	3.4×10^{-5}	10.3×10^{-5}
3	102.65	39.3	1.5×10^{-5}	6.0×10^{-4}	8.50×10^{-5}
3	-52.7	249.3	2.0×10^{-5}	2.0×10^{-4}	5.74×10^{-5}

Composite Nos.

1: Slot cutout foam/embossed mylar at 20 layers/in.
2: Slot cutout foam/embossed mylar/Tissuglas at 19 layers/in.
3: Slot cutout foam/smooth mylar/Tissuglas at 20 layers/in.

Table 5

COMPARISON OF THREE FOAM CUTOUT COMPOSITES AND REGULAR MYLAR/FOAM COMPOSITE

Specimen	Composite	Layer Density (layers/in.)	Room Temperature Conductivity (Btu/hr-ft-^{o}F)
Cutout (No. 1)	Embossed Mylar Cutout Foam	20	17.7×10^{-5}
Cutout (No. 2)	Embossed Mylar Cutout Foam Tissuglas	19	21.2×10^{-5}
Cutout (No. 3)	Smooth Mylar Cutout Foam Tissuglas	20	8.5×10^{-5}
*Regular Mylar/ Foam Composite	Smooth Mylar Solid Foam	23	$8\text{-}8.5 \times 10^{-5}$

*Fully outgassed

Table 6

THERMAL CONDUCTIVITY OF EMBOSSED MYLAR/TISSUGLAS COMPOSITE AT 62 LAYERS PER INCH AT DIFFERENT TEMPERATURES

Mean Insulation Temperature (^{o}F)	ΔT (^{o}F)	Chamber Pressure (torr)	Thermal Conductivity (Btu/hr-ft-^{o}F)
-114.0	95.3	1.4×10^{-5}	2.12×10^{-5}
-5.4	44.8	5.2×10^{-6}	2.97×10^{-5}
107.7	55.0	7.0×10^{-6}	5.97×10^{-5}
198.7	56.4	3.7×10^{-5}	13.3×10^{-5}

Table 7

ROOM TEMPERATURE THERMAL CONDUCTIVITY OF EMBOSSED MYLAR/TISSUGLAS COMPOSITE AT 62 LAYERS PER INCH AT DIFFERENT PRESSURES

Mean Insulation Temperature (^{o}F)	ΔT (^{o}F)	Chamber Pressure	Thermal Conductivity (Btu/hr-ft-^{o}F)
107.7	55.0	7.0×10^{-6} torr	5.97×10^{-5}
108.25	54.5	1.6×10^{-2} torr	3.04×10^{-4}
100.25	16.5	1.8 torr	3.95×10^{-2}
95.75	8.9	1 atm	8.10×10^{-2}

Table 8

DATA POINTS FOR EMBOSSED MYLAR/NYLON NET SPECIMEN ESTABLISHING CONDUCTIVITY AS A FUNCTION OF TEMPERATURE

Mean Insulation Temperature (^{o}F)	ΔT (^{o}F)	Chamber Pressure (torr)	Thermal Conductivity (Btu/hr-ft-^{o}F) ($\times 10^{5}$)
-105.8	53.3	1.6×10^{-5}	4.2
33.8	119.6	4×10^{-5}	10.42
103.65	49.3	1.6×10^{-5}	9.92
204.25	43.5	3.5×10^{-5}	20.7

Table 9

ROOM TEMPERATURE DATA POINTS FOR EMBOSSED MYLAR/NYLON NET SPECIMEN ESTABLISHING ROOM TEMPERATURE CONDUCTIVITY AS A FUNCTION OF PRESSURE

Mean Insulation Temperature (^{o}F)	ΔT (^{o}F)	Chamber Pressure (torr)	Thermal Conductivity (Btu/hr-ft-^{o}F)
103.65	49.3	1.6×10^{-5}	9.92×10^{-5}
89.95	27.3	3.2×10^{-2}	9.94×10^{-4}
91.95	14.1	1.3	1.218×10^{-2}
91.3	14.6	760	1.84×10^{-2}

Table 10

THERMAL CONDUCTIVITY OF THE SHALLOW DIMPLED DIMPLAR SPECIMEN AT 44 LAYERS PER INCH FOR DIFFERENT TEMPERATURES

Mean Insulation Temperature (^{o}F)	ΔT (^{o}F)	Chamber Pressure (torr)	Internal Pressure (torr)	Thermal Conductivity (Btu/hr-ft-^{o}F)
-84.6	43.2	1.0×10^{-5}	2.6×10^{-5}	3.53×10^{-5}
-5.35	49.5	5.4×10^{-6}	2.1×10^{-5}	8.03×10^{-5}
99.6	37.9	1.0×10^{-5}	—	13.2×10^{-5}
208.65	80.9	1.0×10^{-5}	—	24.6×10^{-5}

Table 11

THERMAL CONDUCTIVITY OF SHALLOW DIMPLED DIMPLAR INSULATION COMPOSITE AT 44 LAYERS PER INCH FOR DIFFERENT PRESSURES

Mean Insulation Temperature (^{o}F)	ΔT (^{o}F)	Chamber Pressure (torr)	Thermal Conductivity (Btu/hr-ft-^{o}F)
99.6	37.9	1×10^{-5}	13.2×10^{-5}
107.6	48.2	1×10^{-2}	6.24×10^{-4}
94.85	12.9	1.7	5.32×10^{-2}
89.75	9.3	760	7.44×10^{-2}

Table 12

THERMAL CONDUCTIVITY OF EMBOSSED MYLAR/SILK NET INSULATION COMPOSITE AT 56 LAYERS PER INCH FOR DIFFERENT TEMPERATURES

Mean Insulation Temperature (^{o}F)	ΔT (^{o}F)	Chamber Pressure (torr)	Internal Pressure (torr)	Thermal Conductivity (Btu/hr/ft-^{o}F)
-94.25	50.5	8.4×10^{-6}	1×10^{-5}	2.49×10^{-5}
99.75	36.5	2×10^{-5}	1.2×10^{-4}	11.57×10^{-5}
207.5	48.0	1×10^{-5}	1.5×10^{-4}	15.7×10^{-5}

Table 13

THERMAL CONDUCTIVITY OF EMBOSSED MYLAR/SILK NET INSULATION COMPOSITE AT 56 LAYERS PER INCH FOR DIFFERENT PRESSURES

Mean Insulation Temperature (^{o}F)	ΔT (^{o}F)	Chamber Pressure (torr)	Thermal Conductivity (Btu/hr-ft-^{o}F)
99.75	36.5	2×10^{-5}	11.57×10^{-5}
97.7	33.0	2.2×10^{-2}	1.163×10^{-3}
116.45	41.9	1.0	9.08×10^{-3}
111.35	37.7	760	1.72×10^{-2}

ILLUSTRATIONS

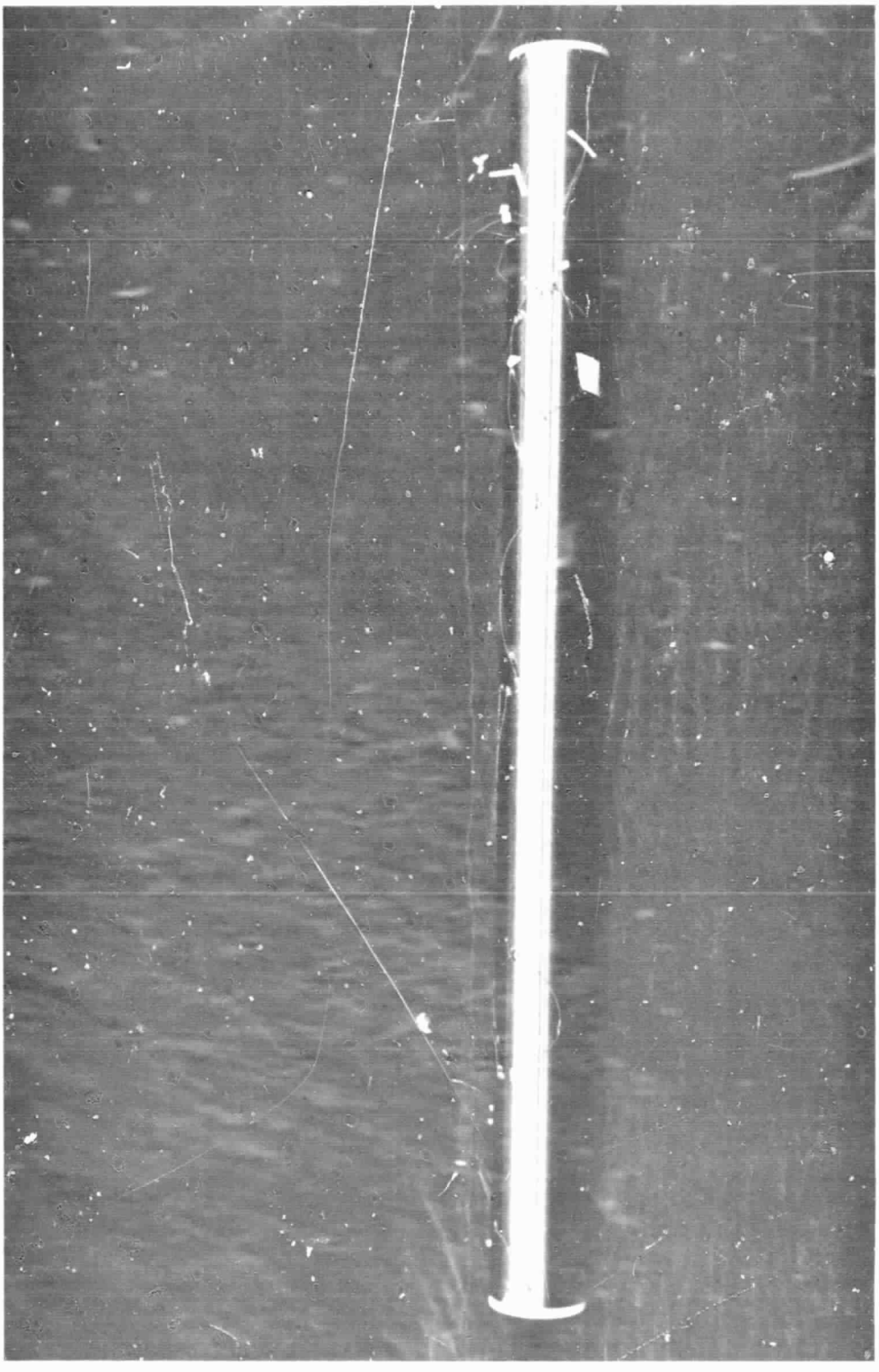

Fig. 1 - Lockheed/Huntsville's Electrical Cylindrical Calorimeter

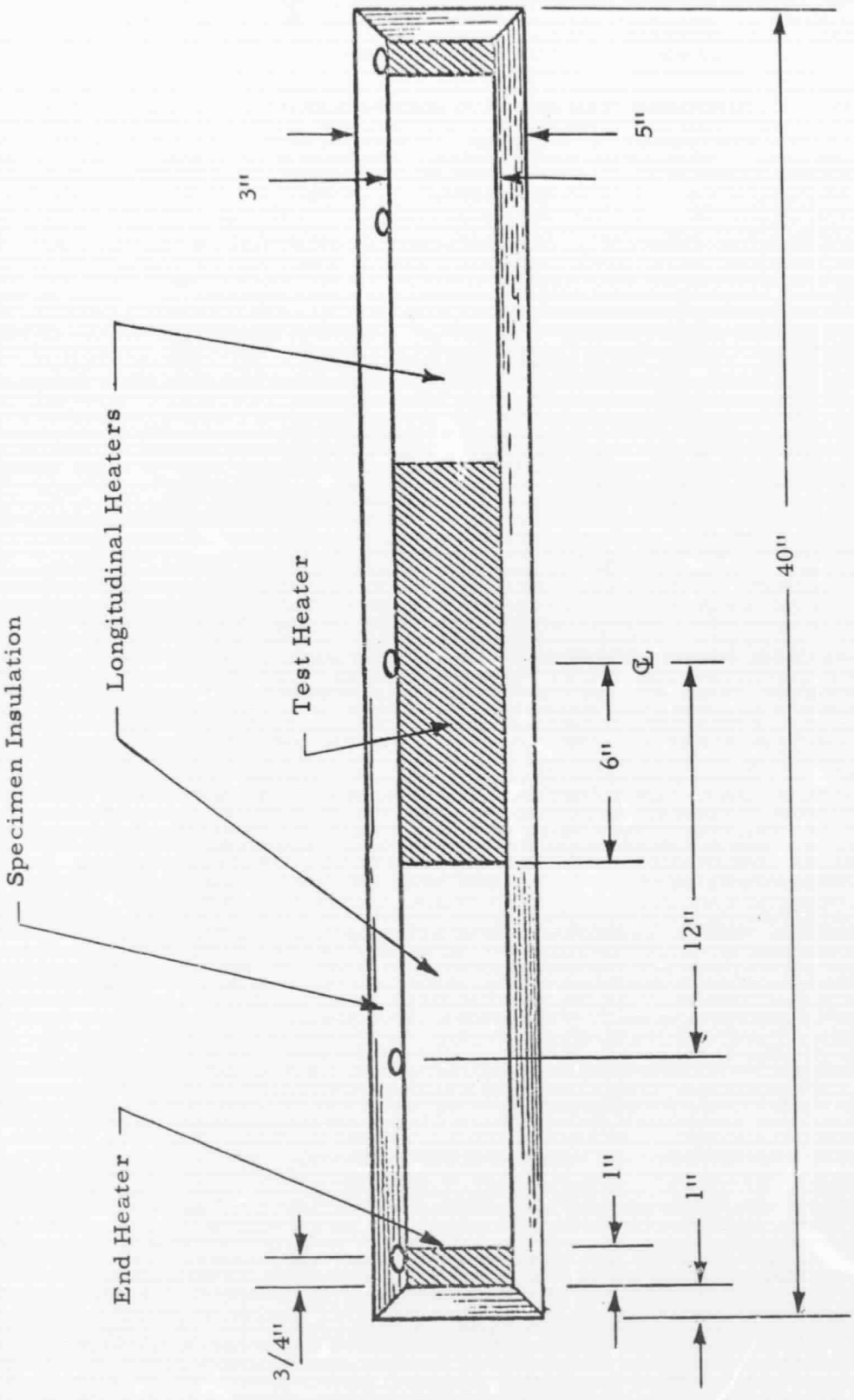

Fig. 2 - Schematic of LMSC/HREC Cylindrical Calorimeter Design

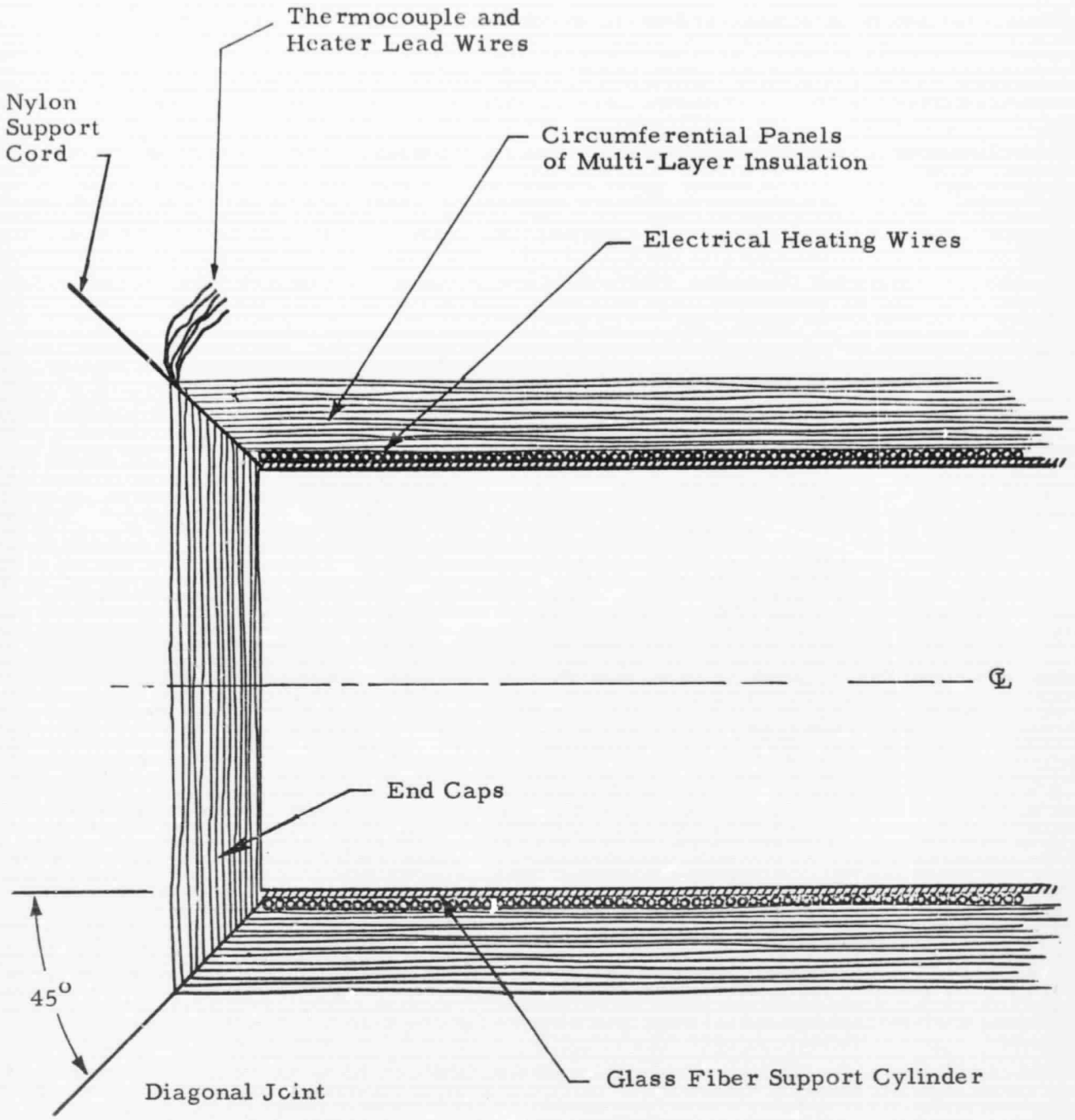

Fig. 3 - Insulation Application Concept

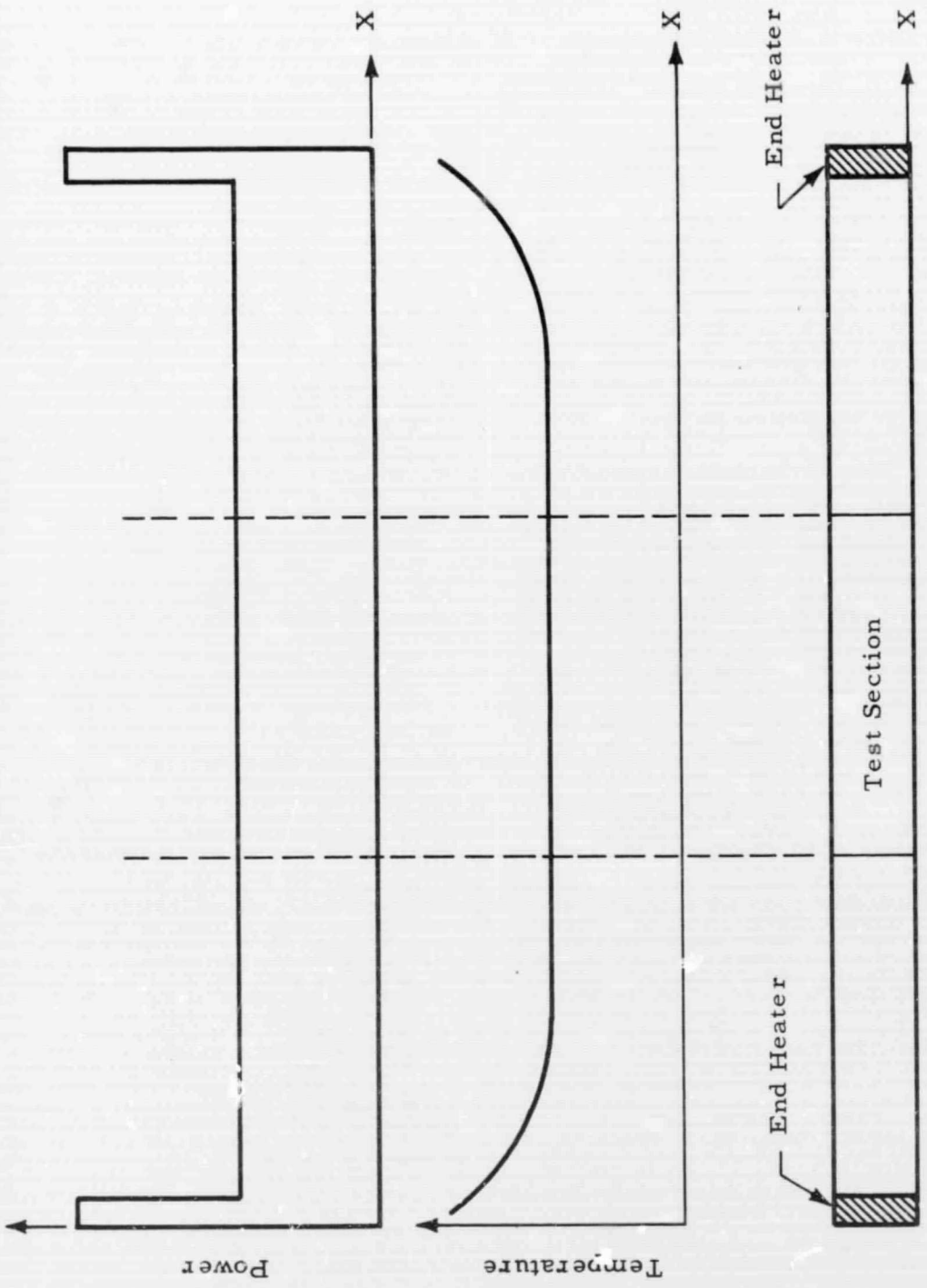

Fig. 4 - Power and Temperature Distributions Along Calorimeter When Data Point is Being Acquired

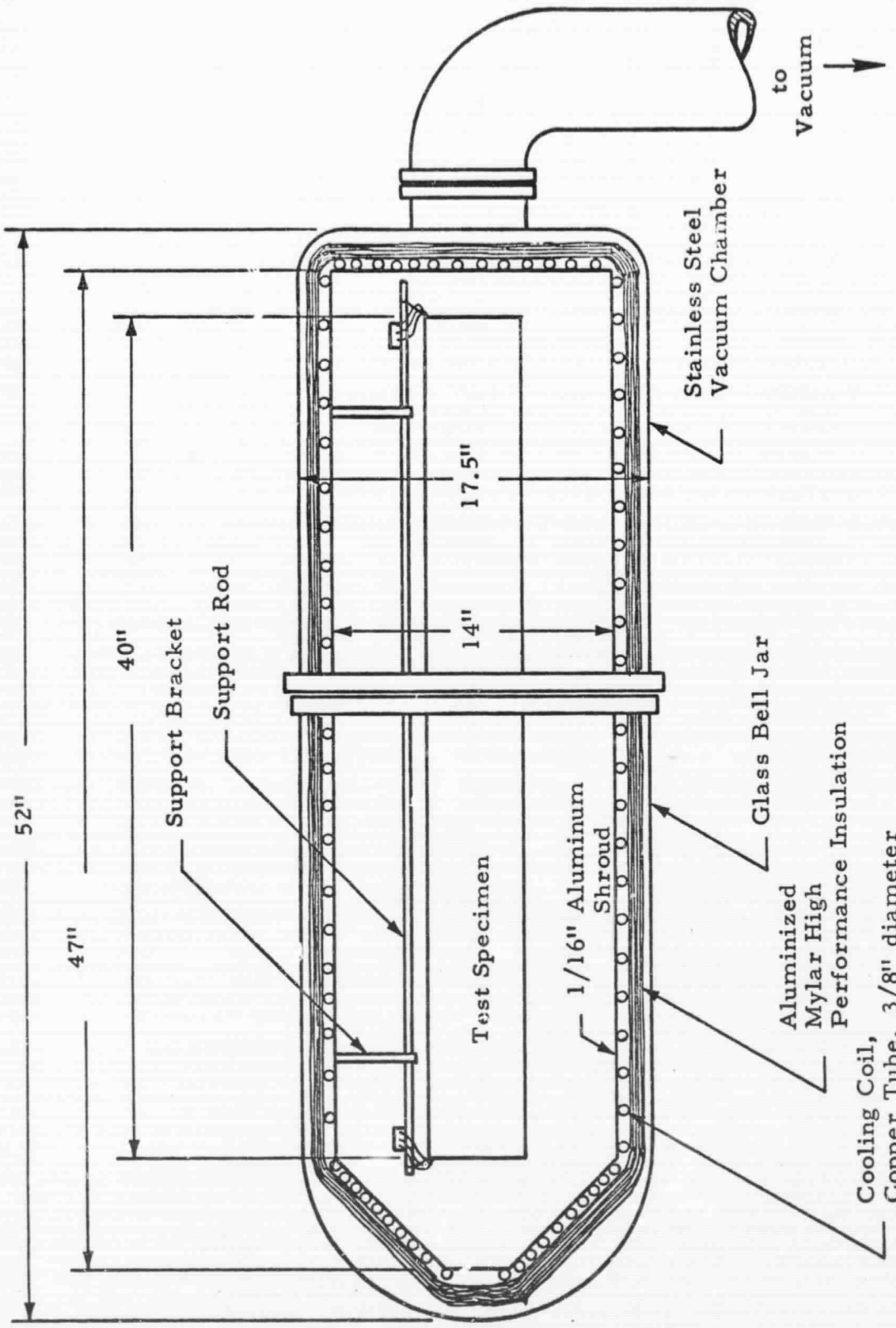

Figure 5 - Environmental Control and Vacuum Chamber System

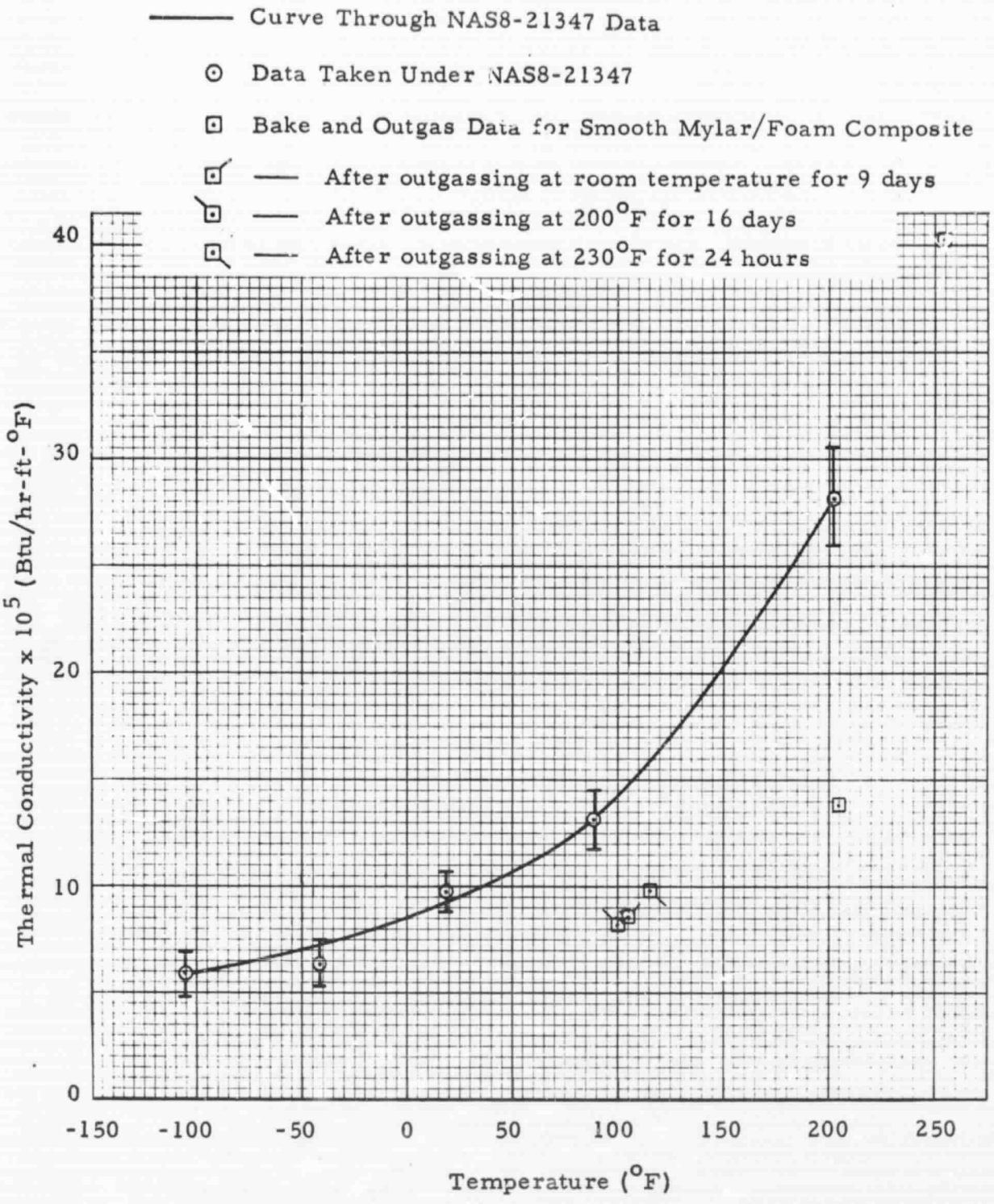

Fig. 6 - Thermal Conductivity for Unperforated 1/4-Mil Double-Aluminized Mylar and Red Polyurethane Foam With and Without Cutouts

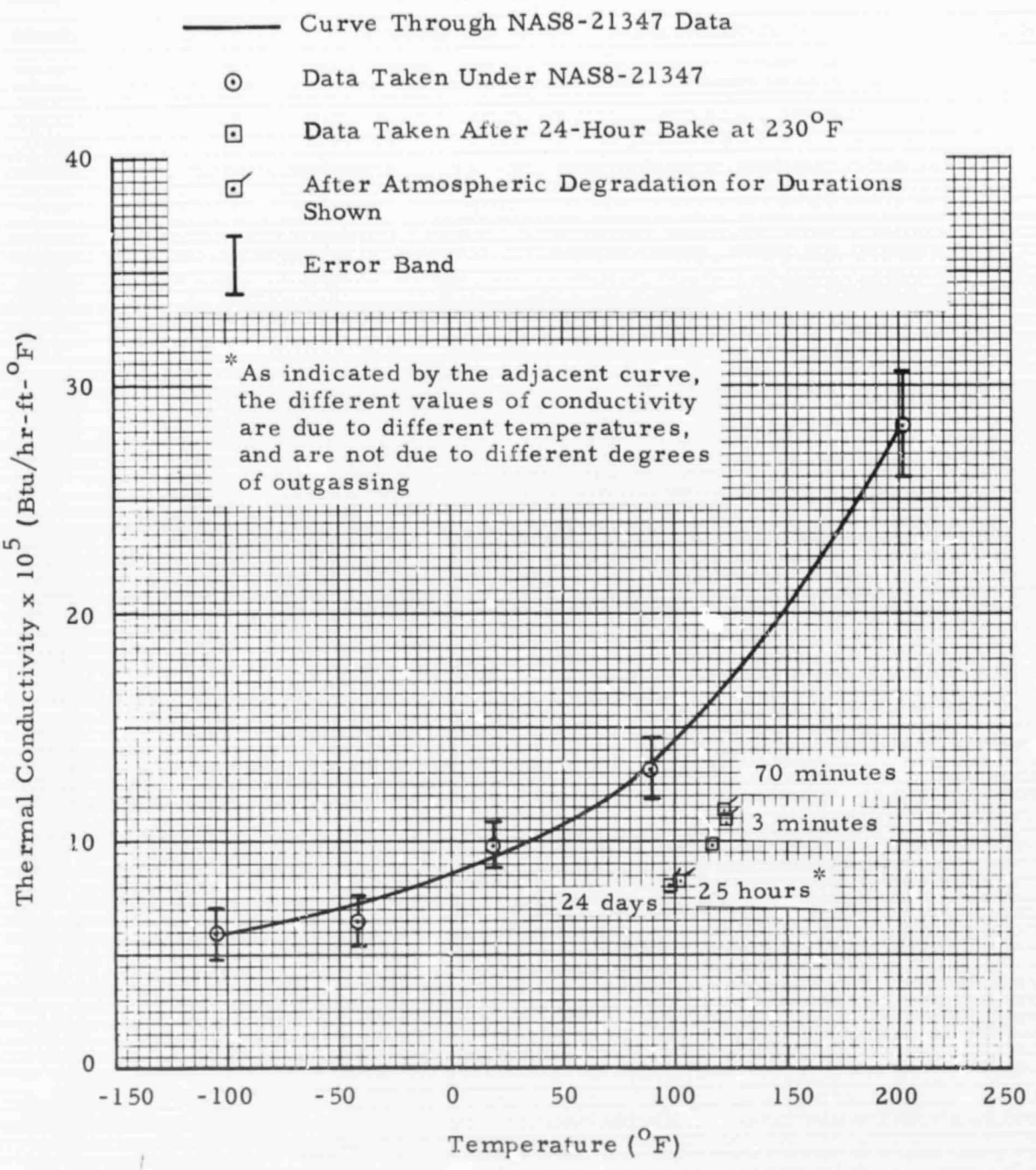

Fig. 7 - Thermal Conductivity for Unperforated 1/4-Mil Double Aluminized Mylar and Red Polyurethane Foam Showing the Effect of Atmospheric Exposure to Thermal Conductivity

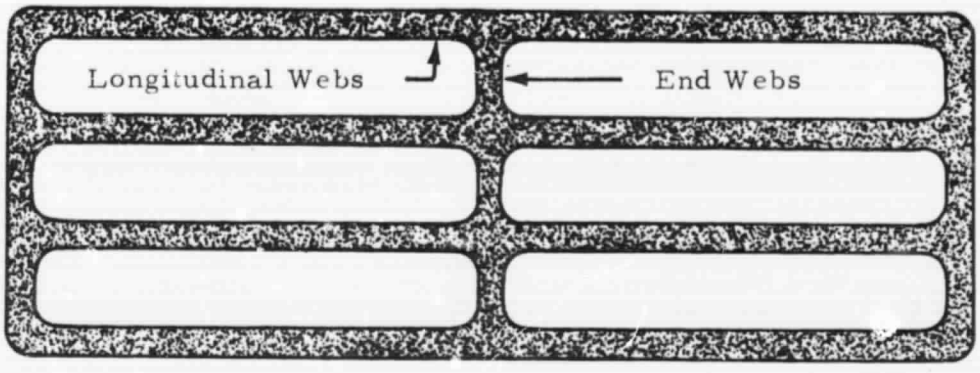

Fig. 8 - Rounded-Corner Slot Cutout

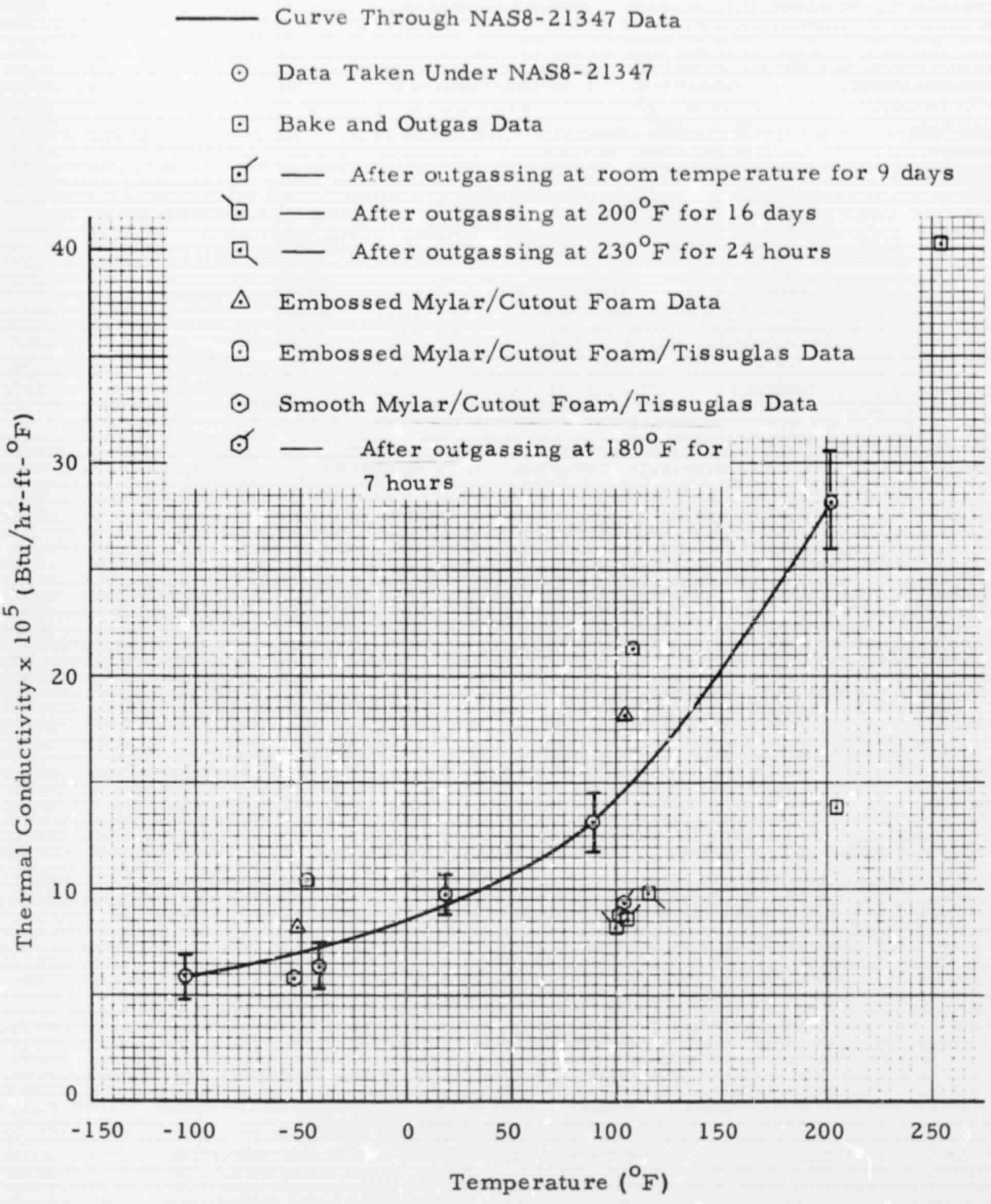

Fig. 9 - Thermal Conductivity for Unperforated 1/4-Mil Double-Aluminized Mylar and Red Polyurethane Foam With and Without Cutouts

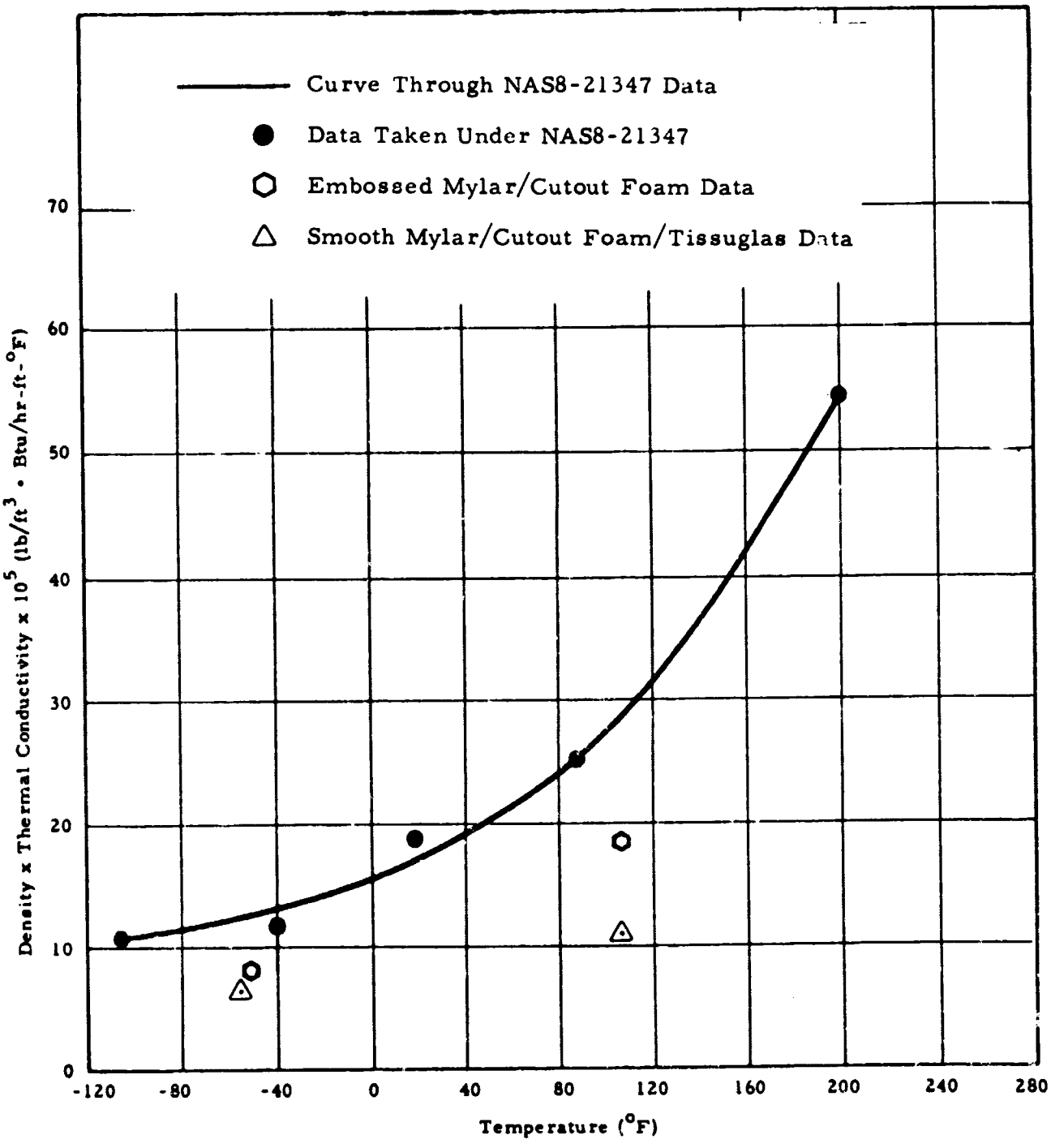

Fig. 10 - Density x Thermal Conductivity – Unperforated 1/4-mil Double-Aluminized Mylar and Red Polyurethane Foam With and Without Cutouts

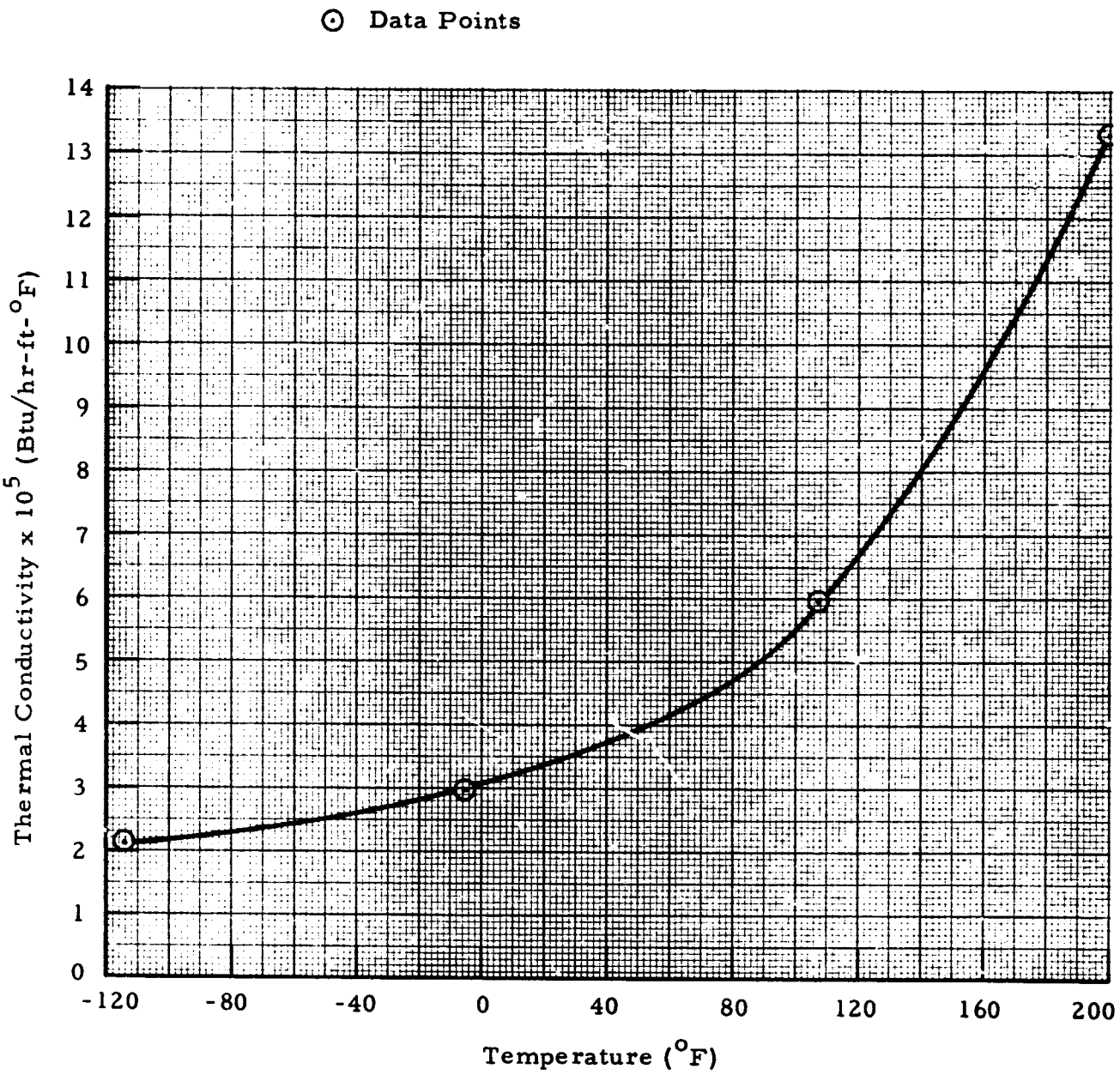

Fig. 11 - Thermal Conductivity – Embossed Mylar/Tissuglas at 62 Layers per Inch

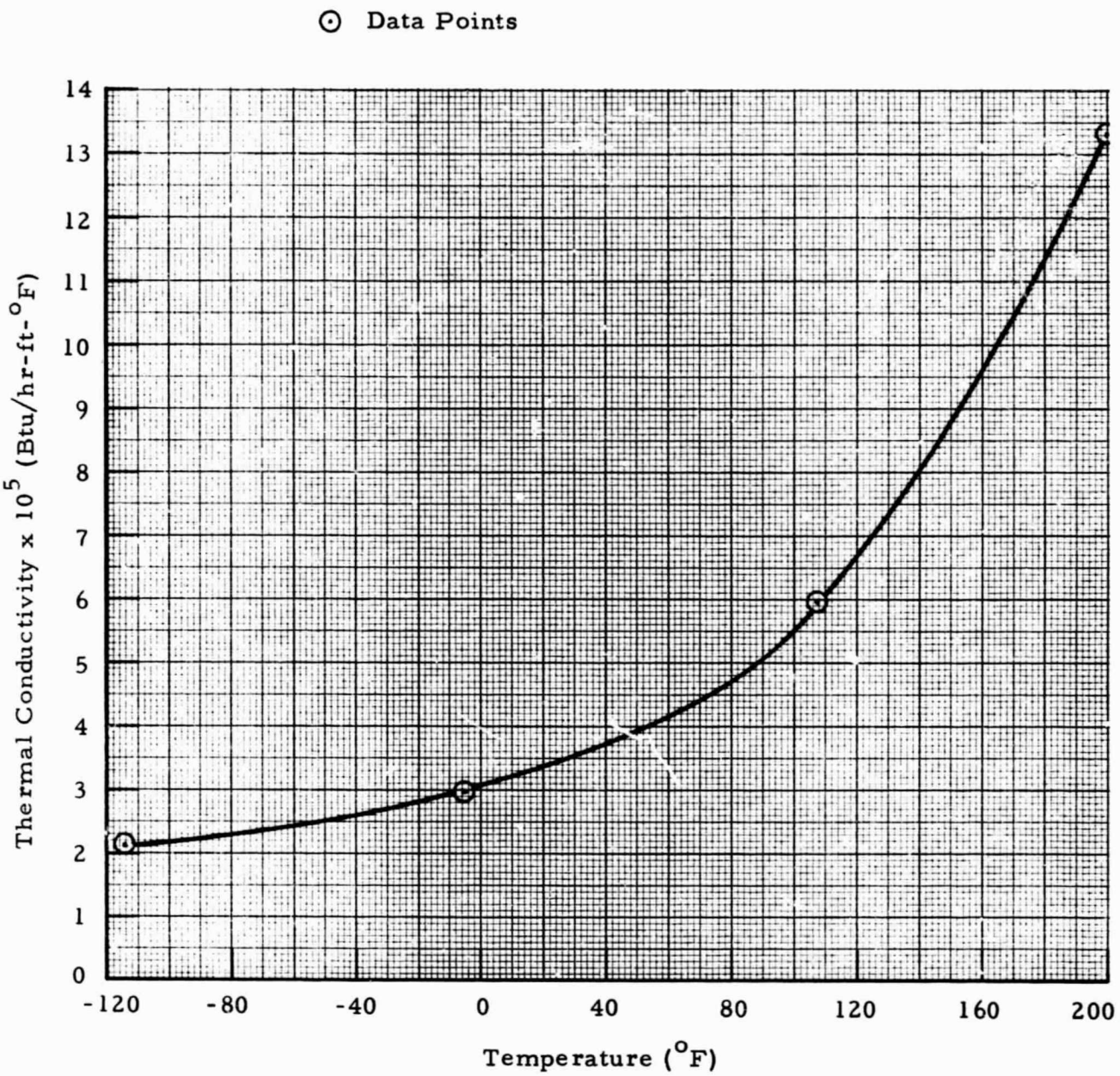

Fig. 11 - Thermal Conductivity – Embossed Mylar/Tissuglas at 62 Layers per Inch

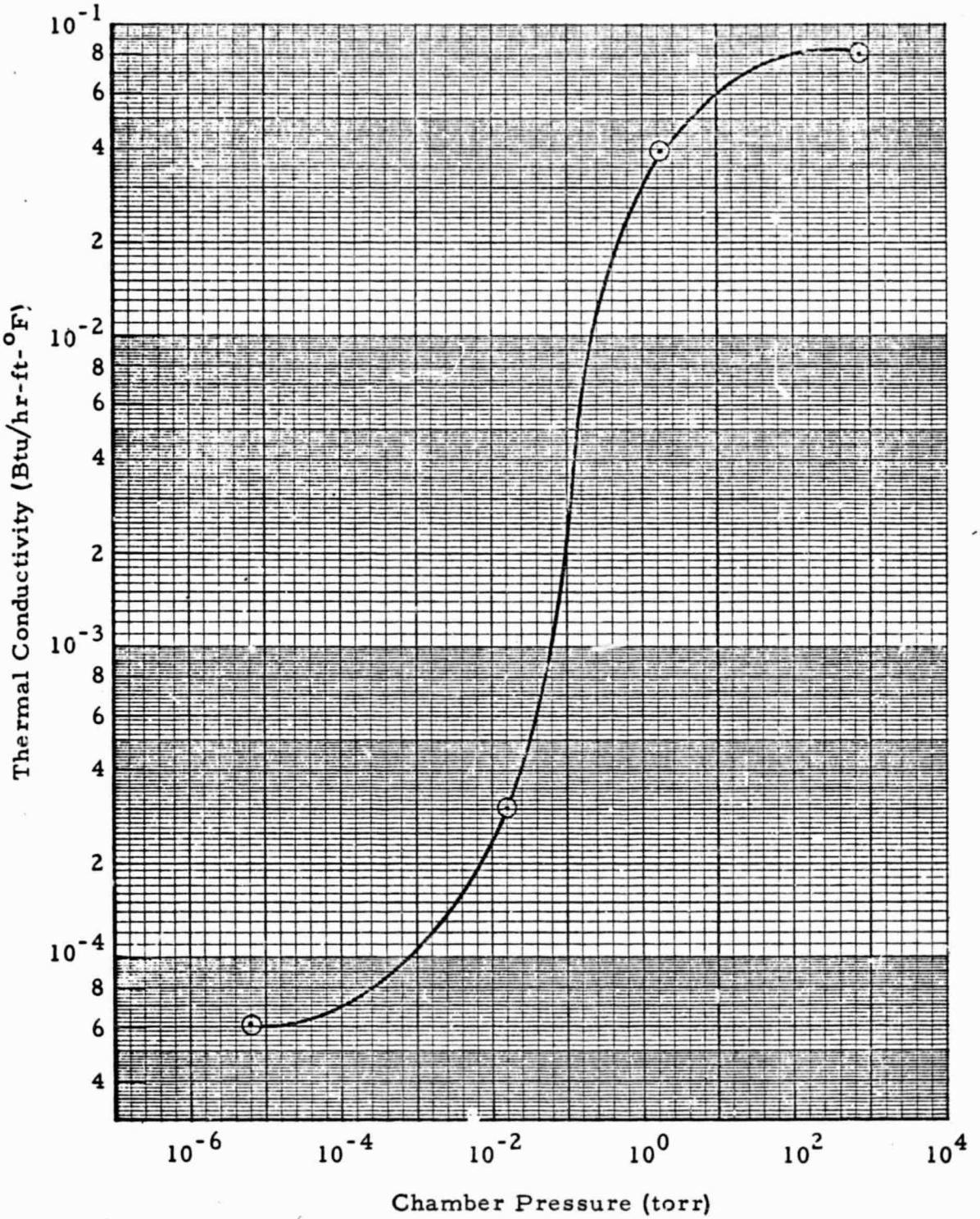

Fig. 12 - Thermal Conductivity -- Embossed Mylar/ Tissuglas Insulation Composite at Room Temperature

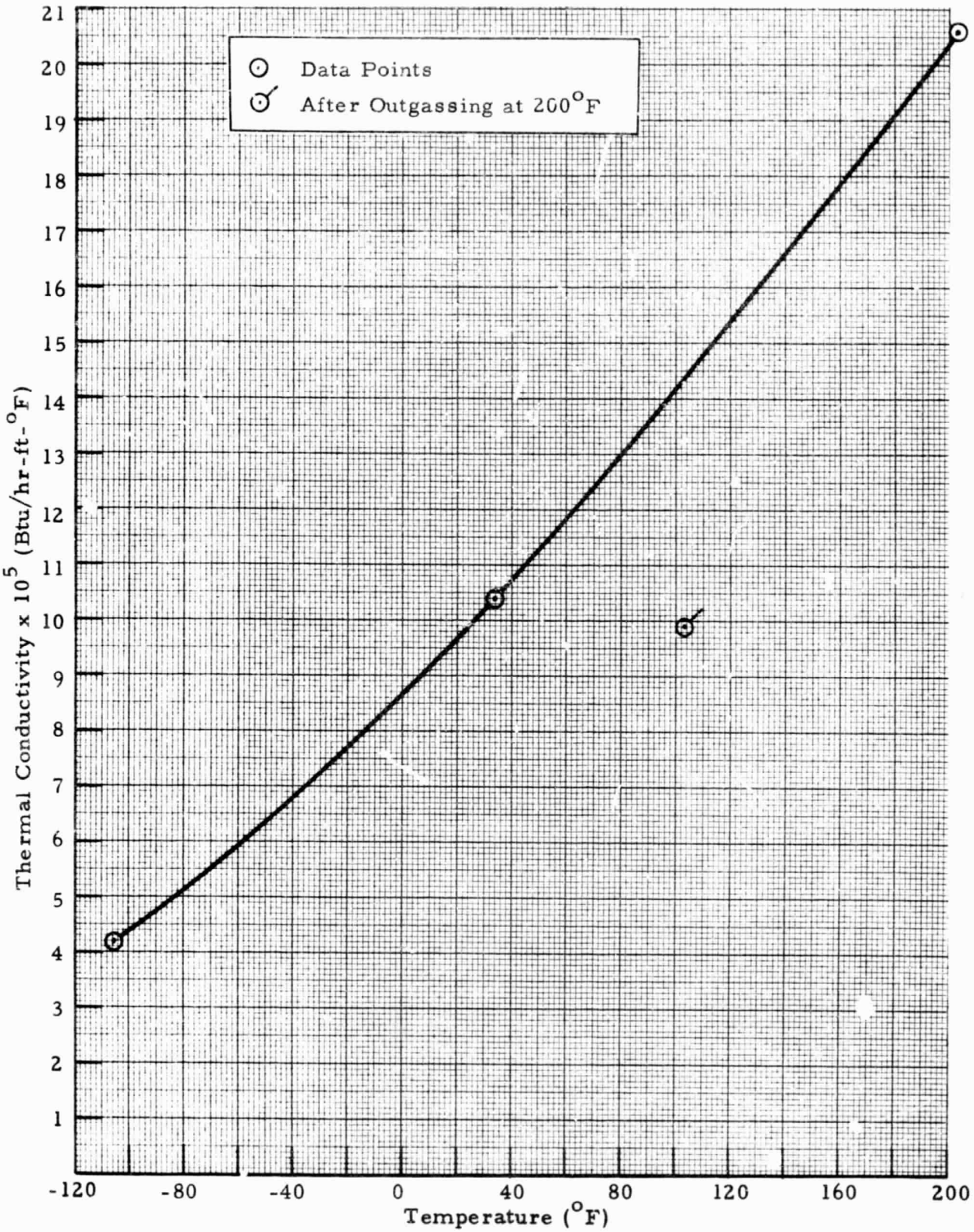

Fig. 13 - Thermal Conductivity – Embossed Mylar/ Nylon Net at 50 Layers per Inch

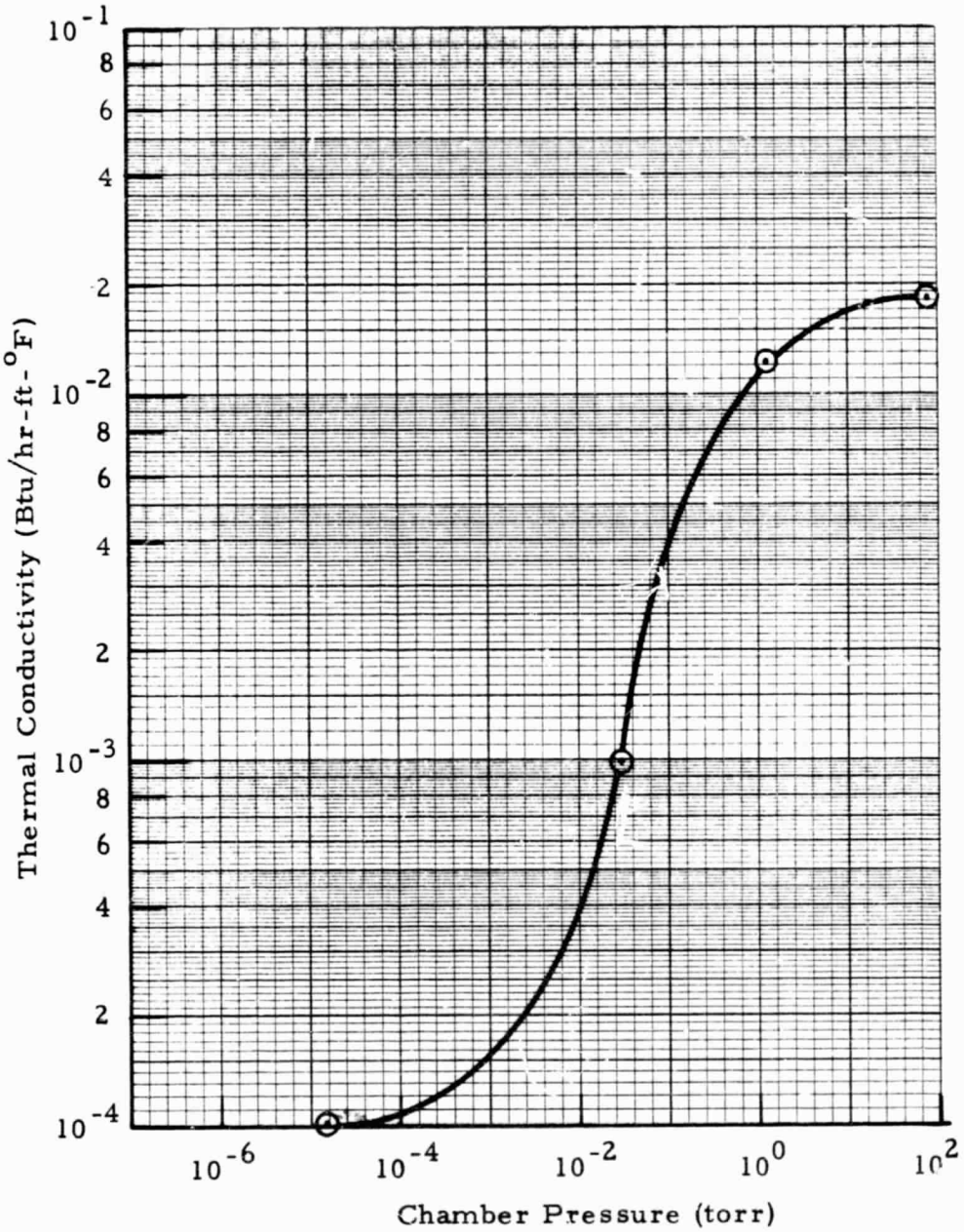

Fig. 14 - Thermal Conductivity – Embossed Mylar/Nylon Net Insulation Composite at Room Temperature

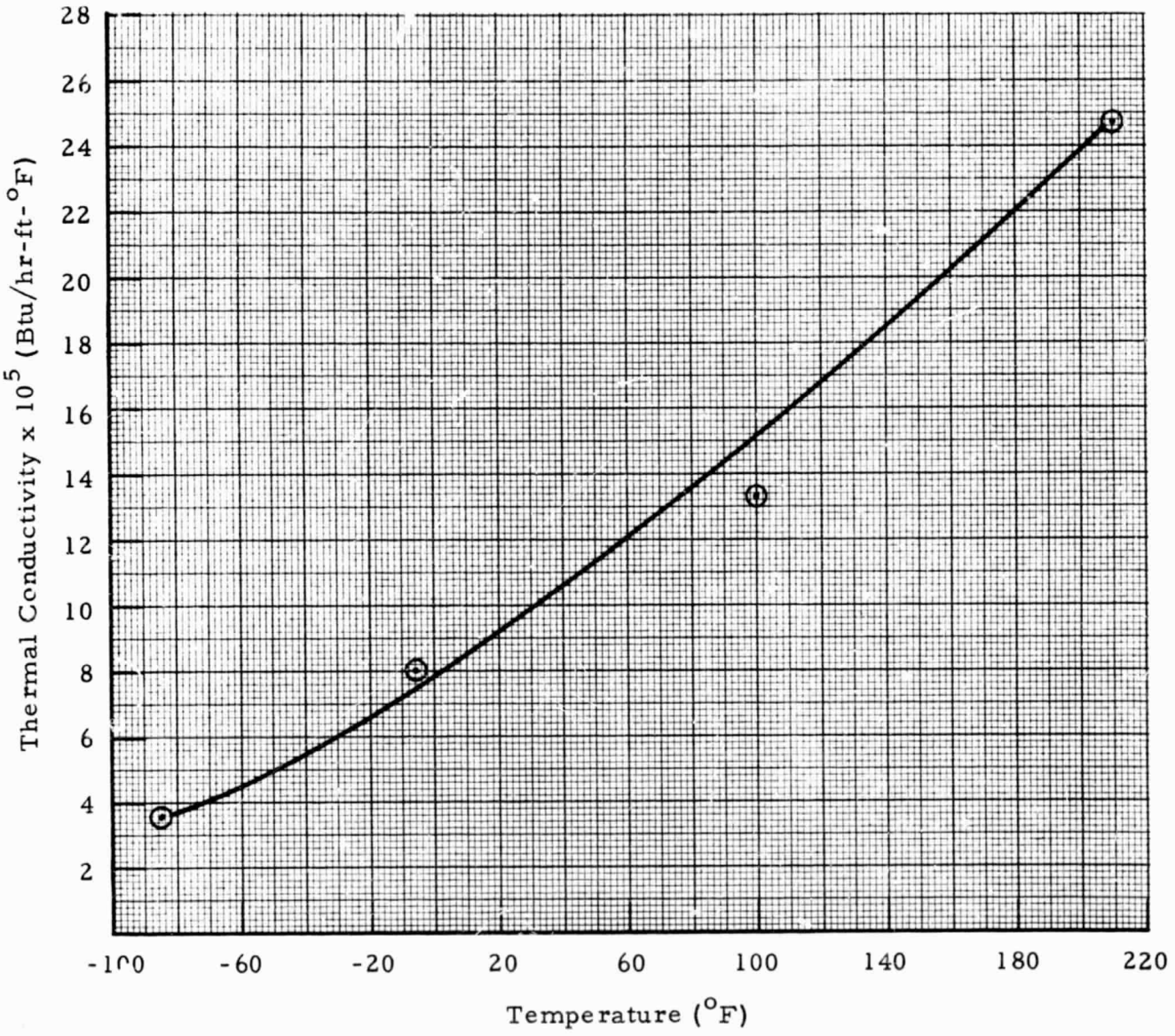

Fig. 15 - Thermal Conductivity for Shallow Dimpled Dimplar at 44 Layers per Inch

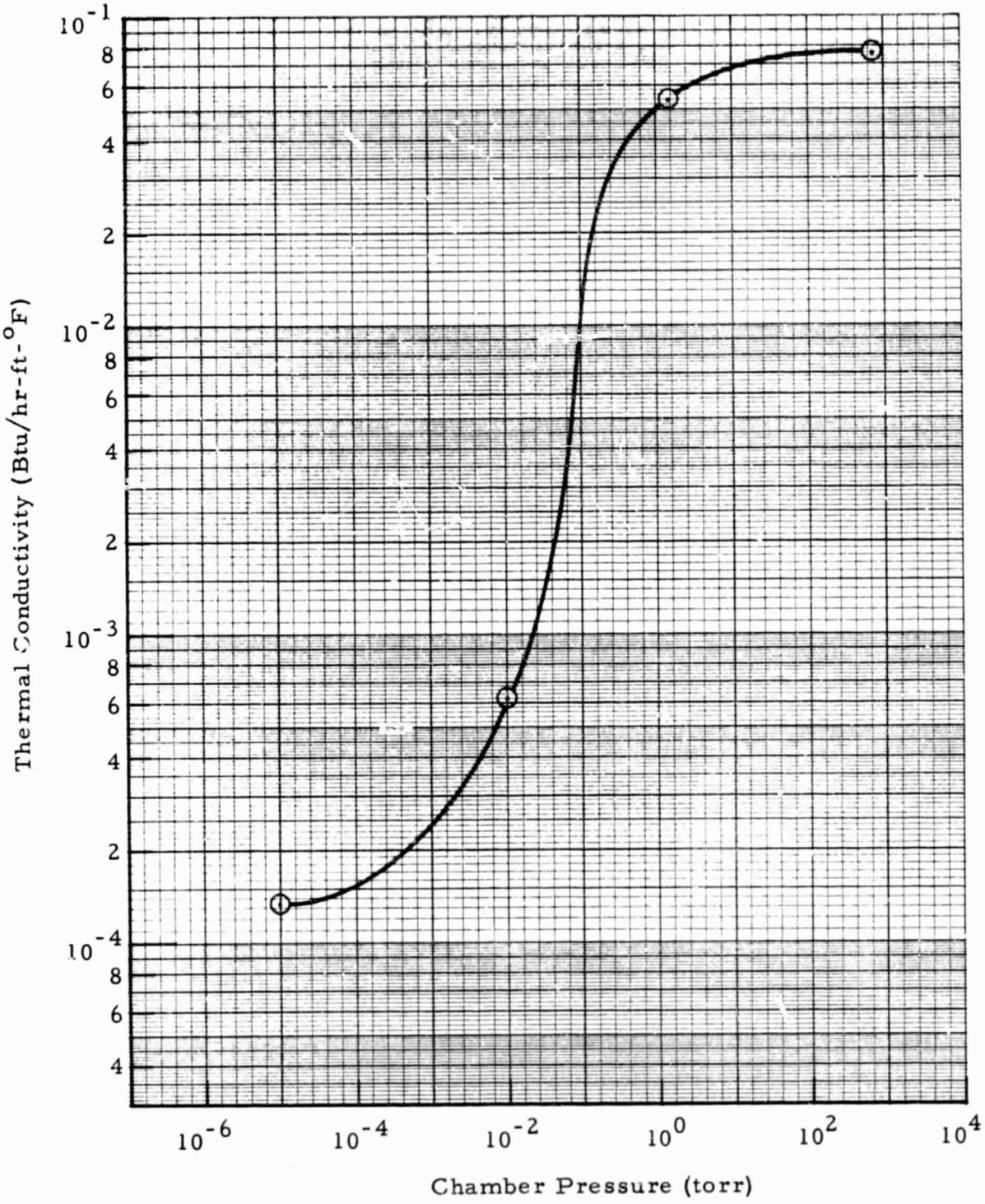

Fig. 16 - Thermal Conductivity – Shallow Dimpled Dimplar Insulation Composite at 44 Layers per Inch at Room Temperature

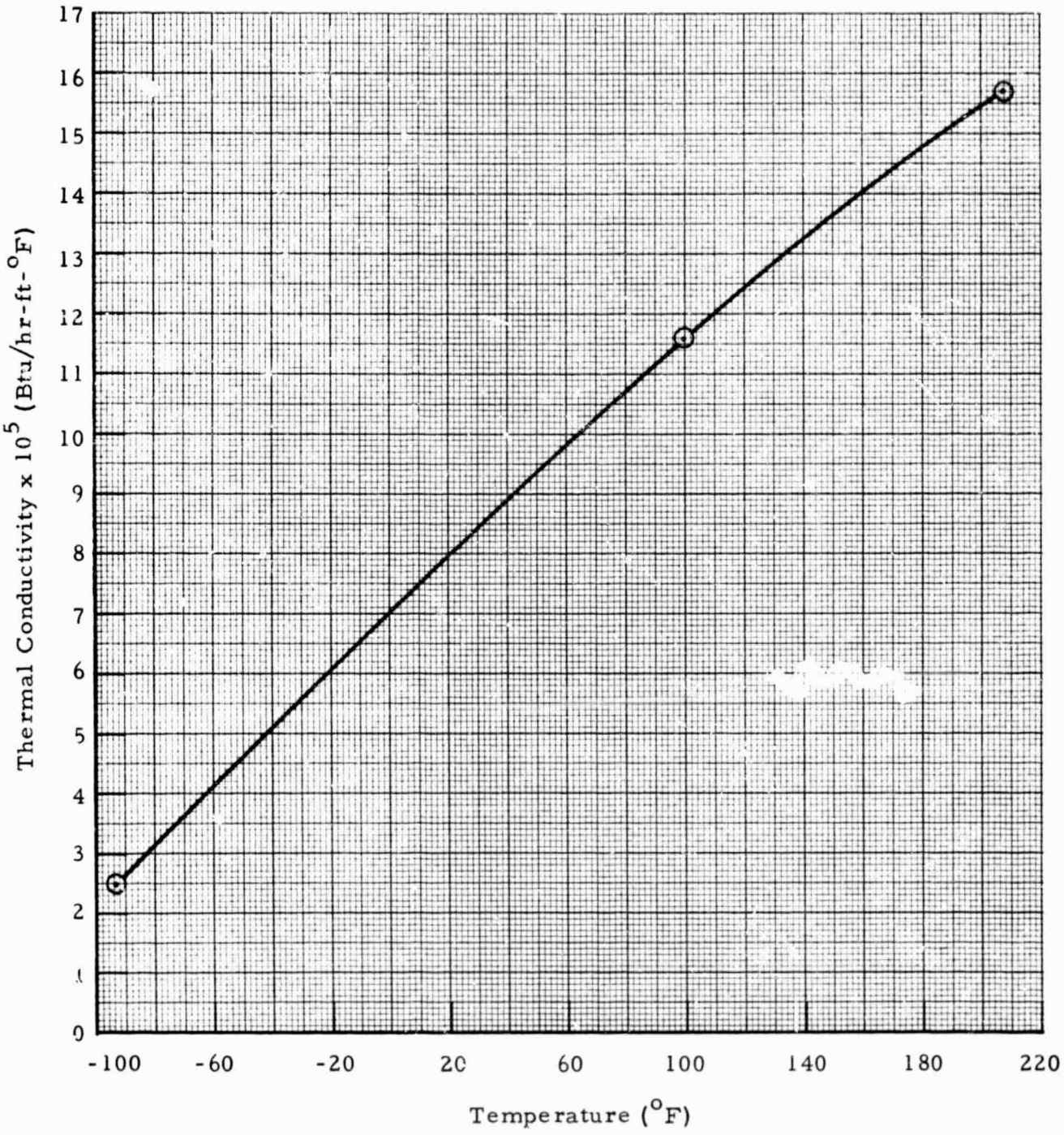

Fig. 17 - Thermal Conductivity — Embossed Mylar/Silk Net at 56 Layers per Inch

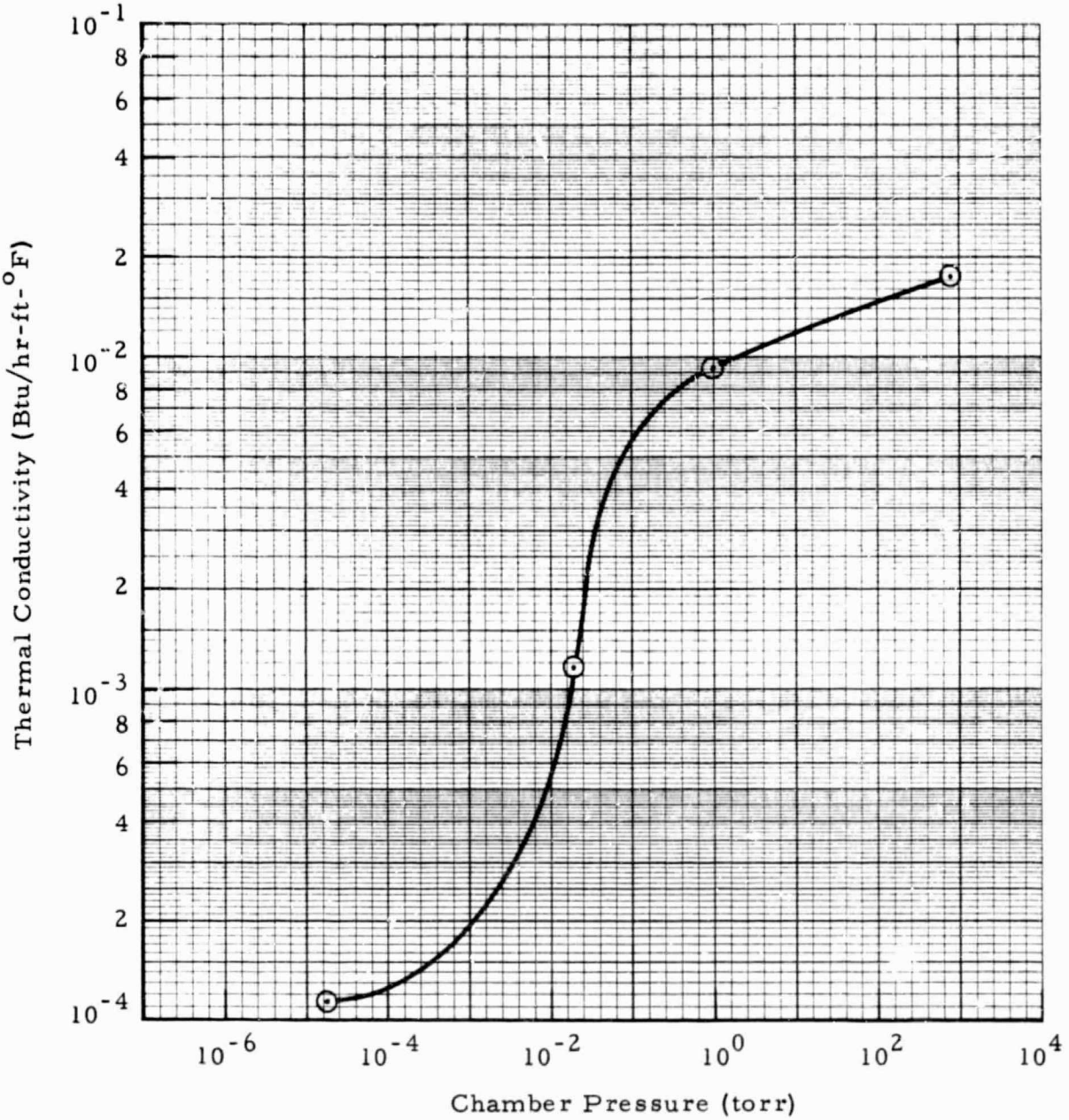

Fig. 18 - Thermal Conductivity – Embossed Mylar/Silk Net Insulation Composite at Room Temperature

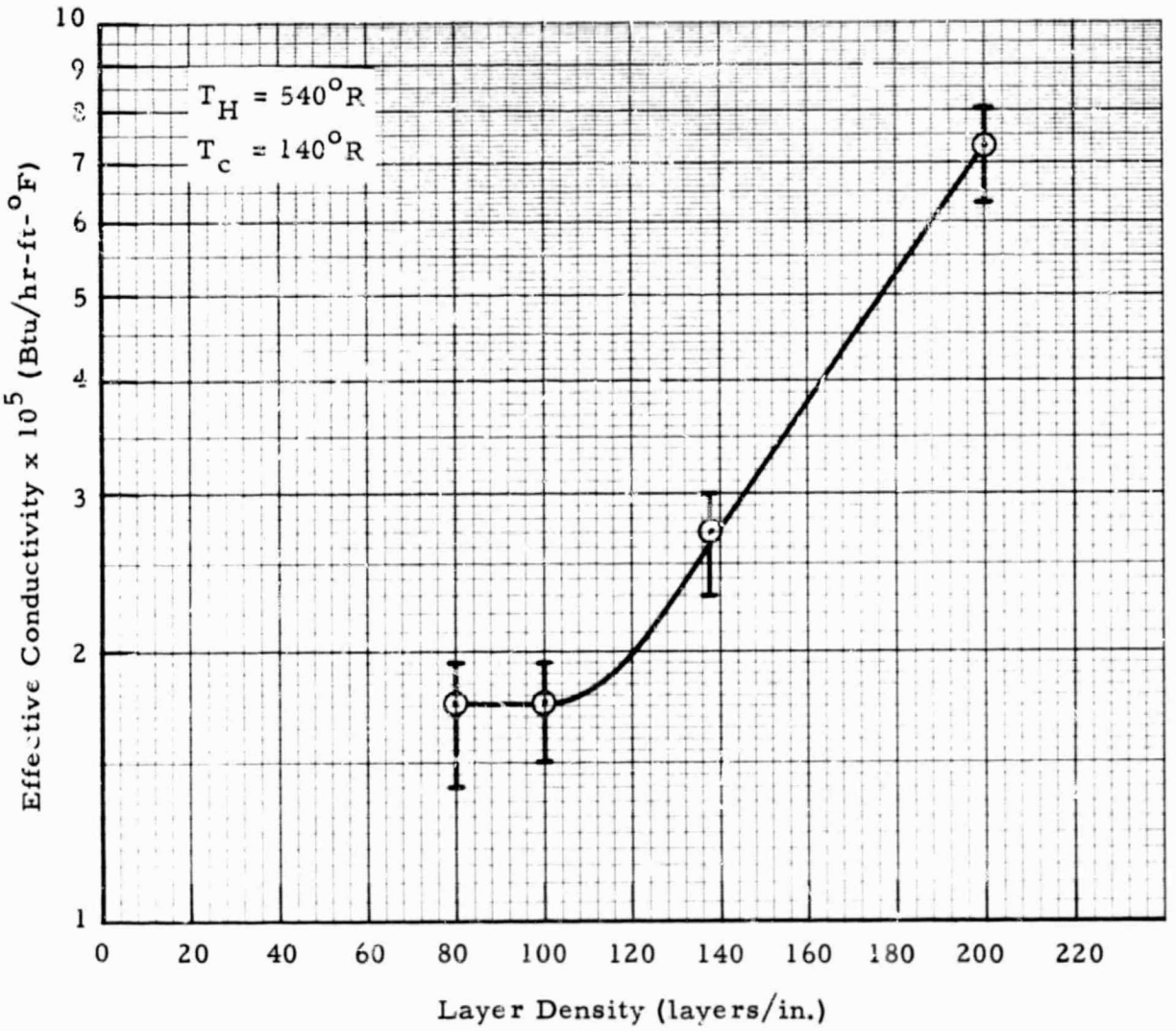

Fig. 19 - Effective Conductivity of Double-Aluminized Mylar/Nylon Net Composite Measured by Lockheed/Sunnyvale (Ref. 2)

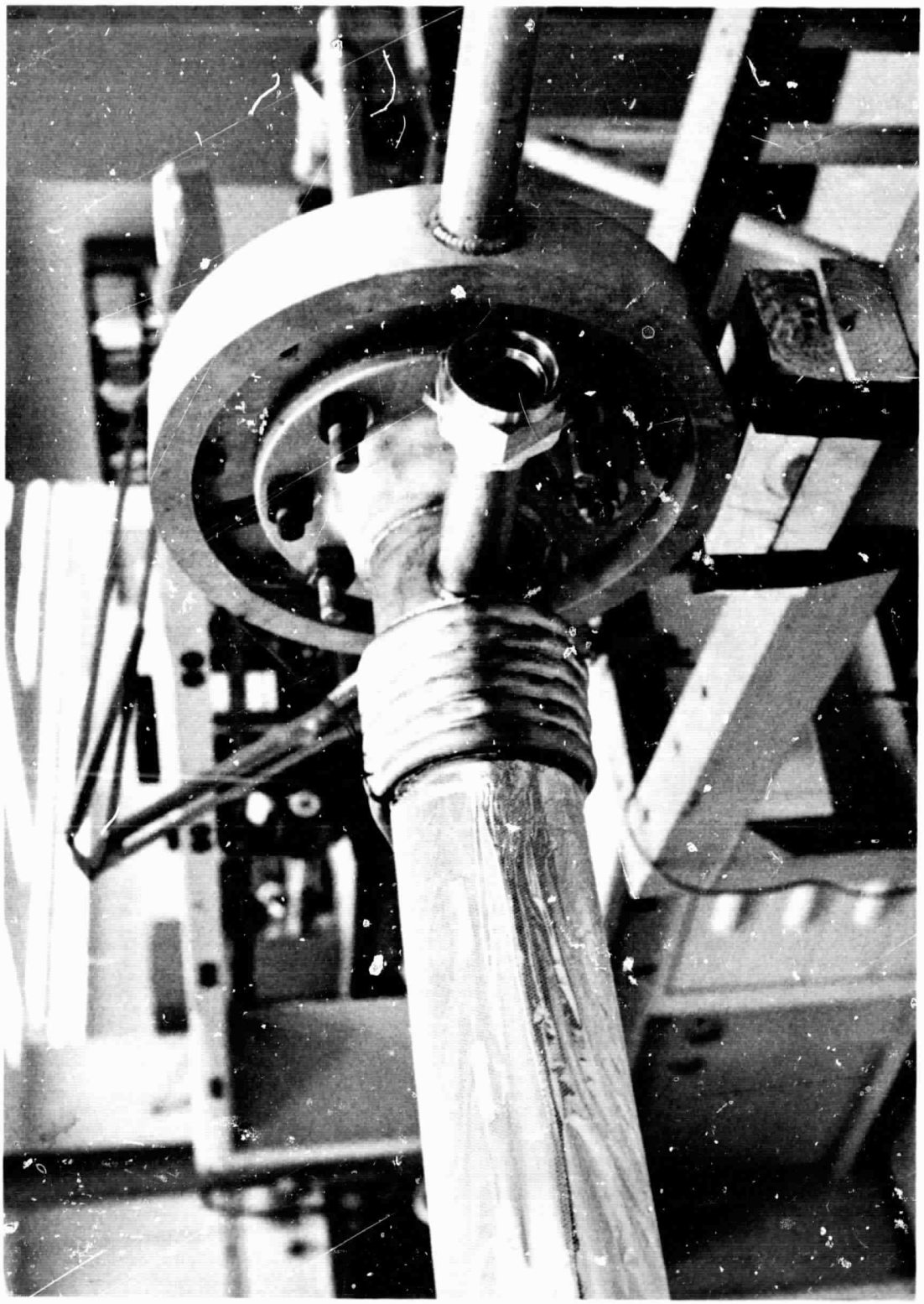

Fig. 20 - Cooling Coil on Tank Neck

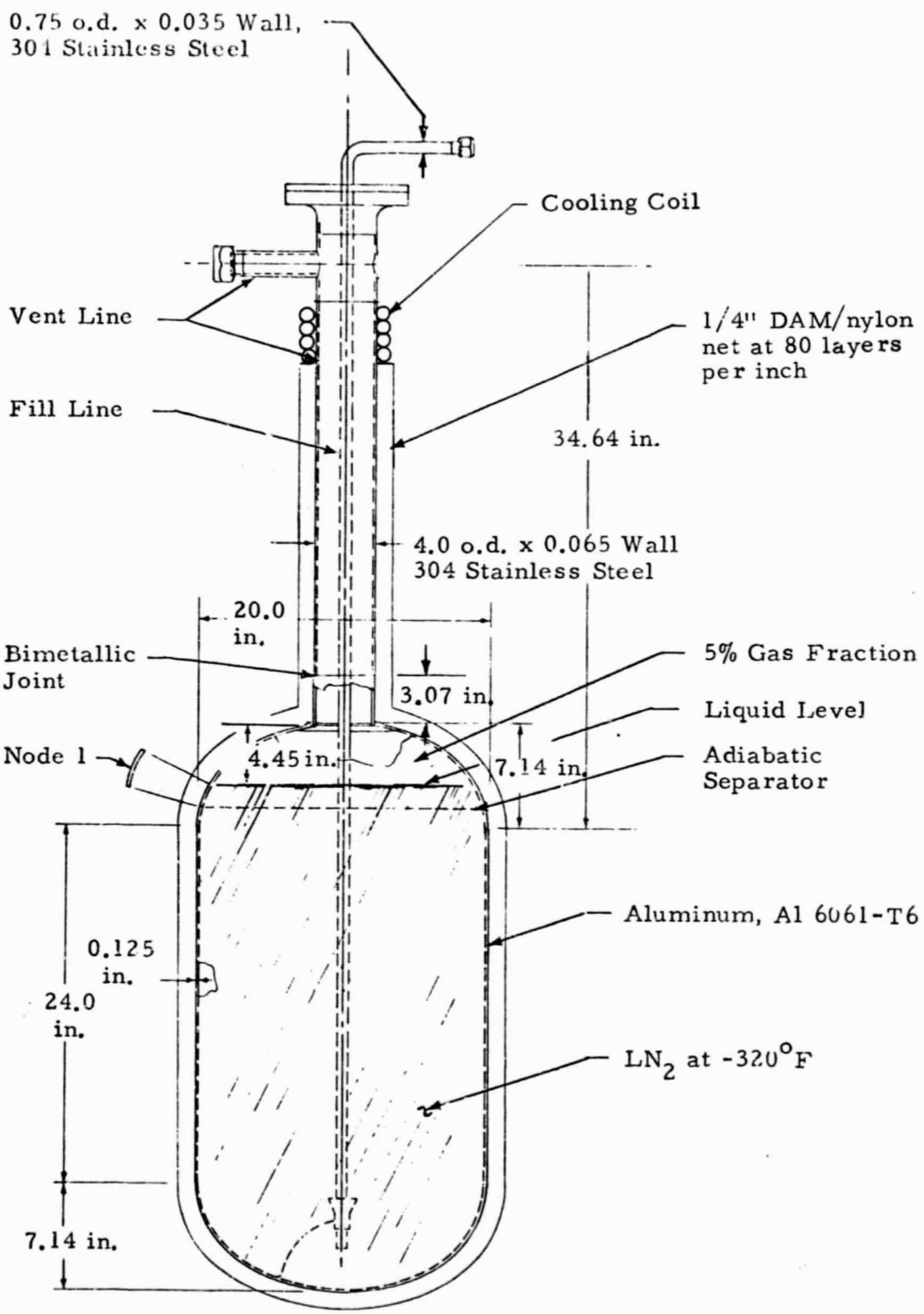

Fig. 21 - Schematic of MSFC 20-Inch Cryogenic Tank

Fig. 22 - Tank During Wrapping Process Showing Mylar Lunes To Be Applied to End of Tank

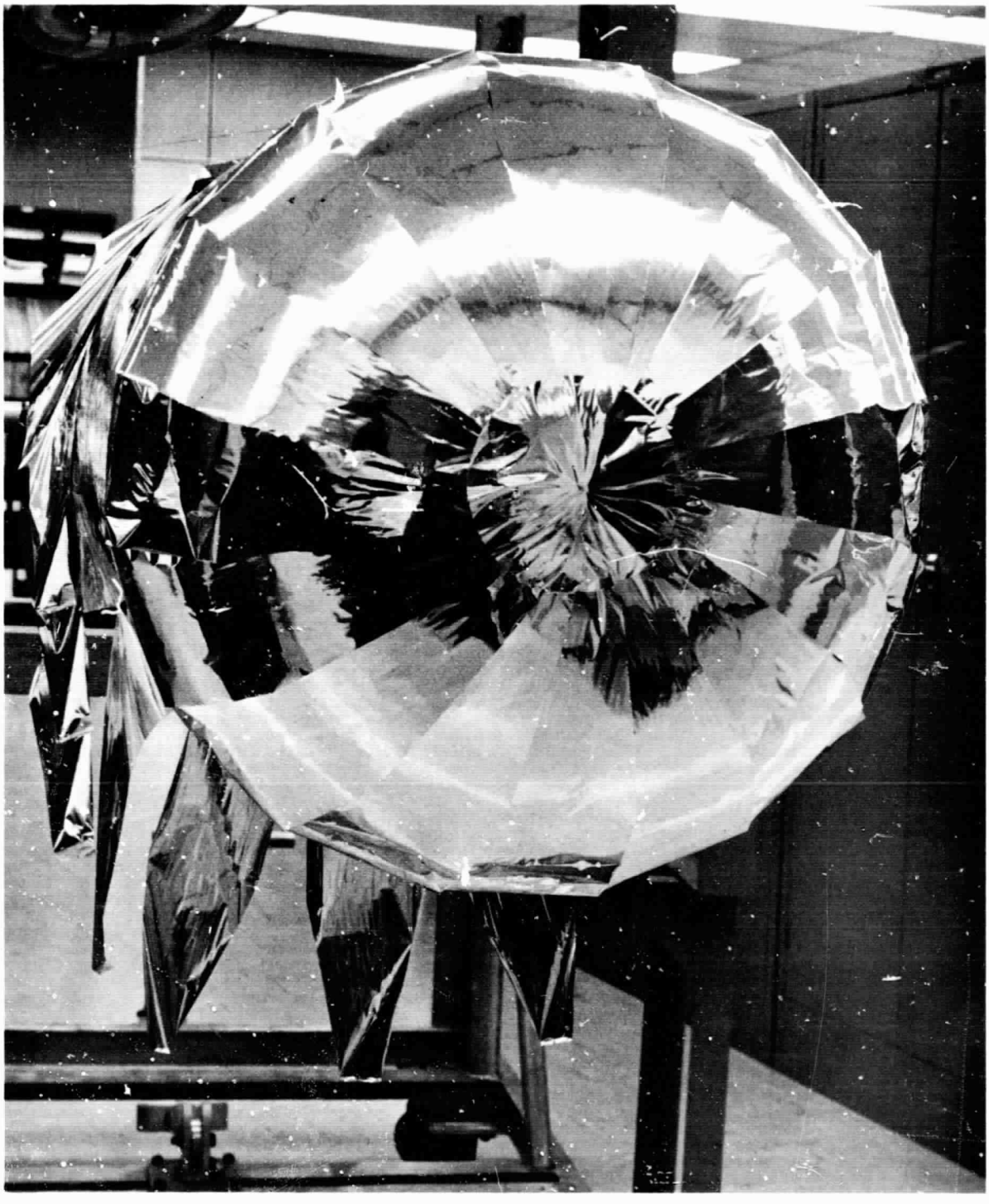

Fig. 23 - Tank During Wrapping Process Showing Completed Mylar End Layer

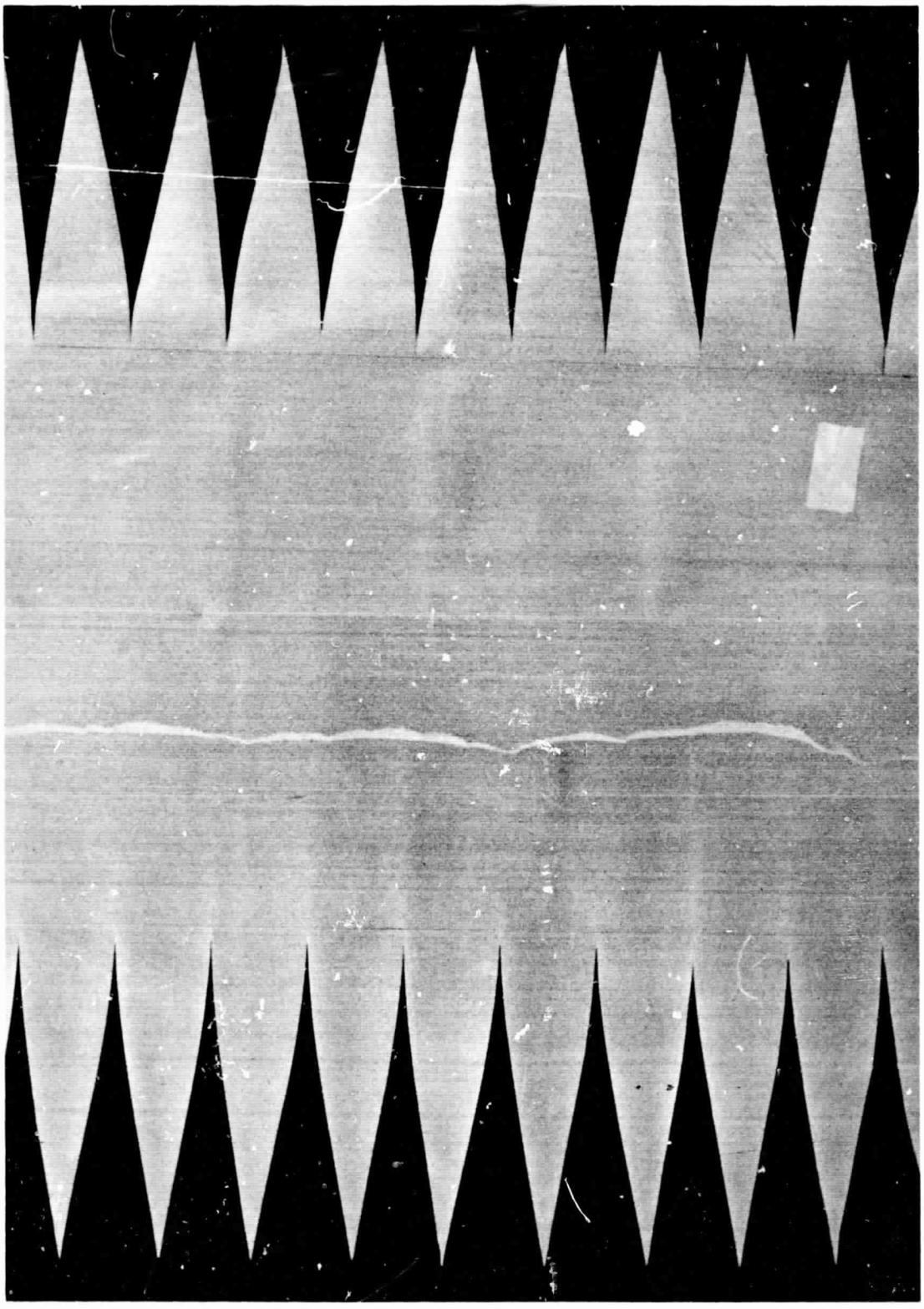

Fig. 24 - Nylon Net Insulation Layer Prior to Application on Tank Showing Geometry of Ellipsoidal Lunes

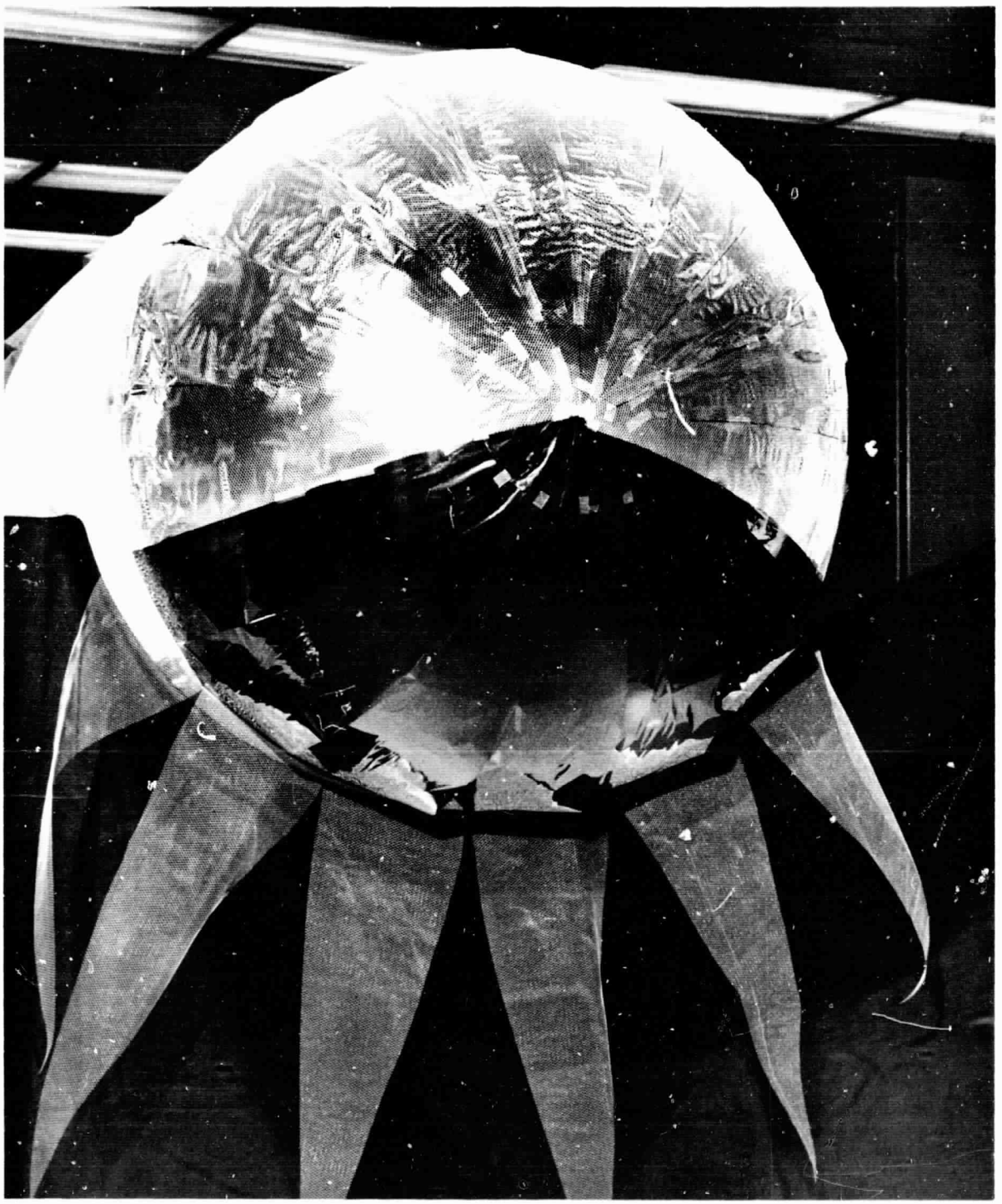

Fig. 25 - Tank During Wrapping Process Showing Application of Nylon Lunes on End of Tank

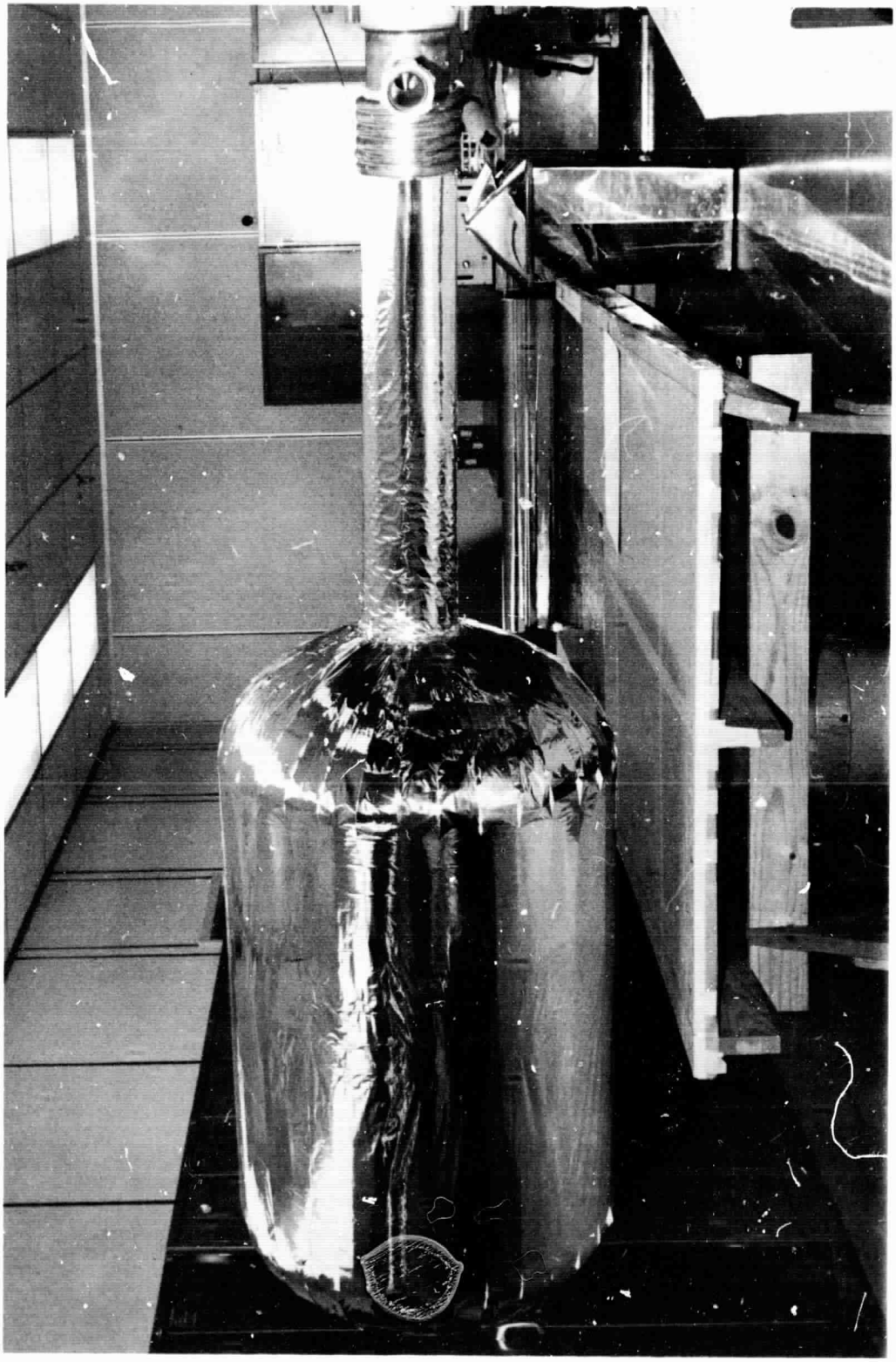

Fig. 26 - Tank Insulated with 21 Layers of Mylar and 20 Layers of Nylon Net Applied with Thickness of 1/4 Inch

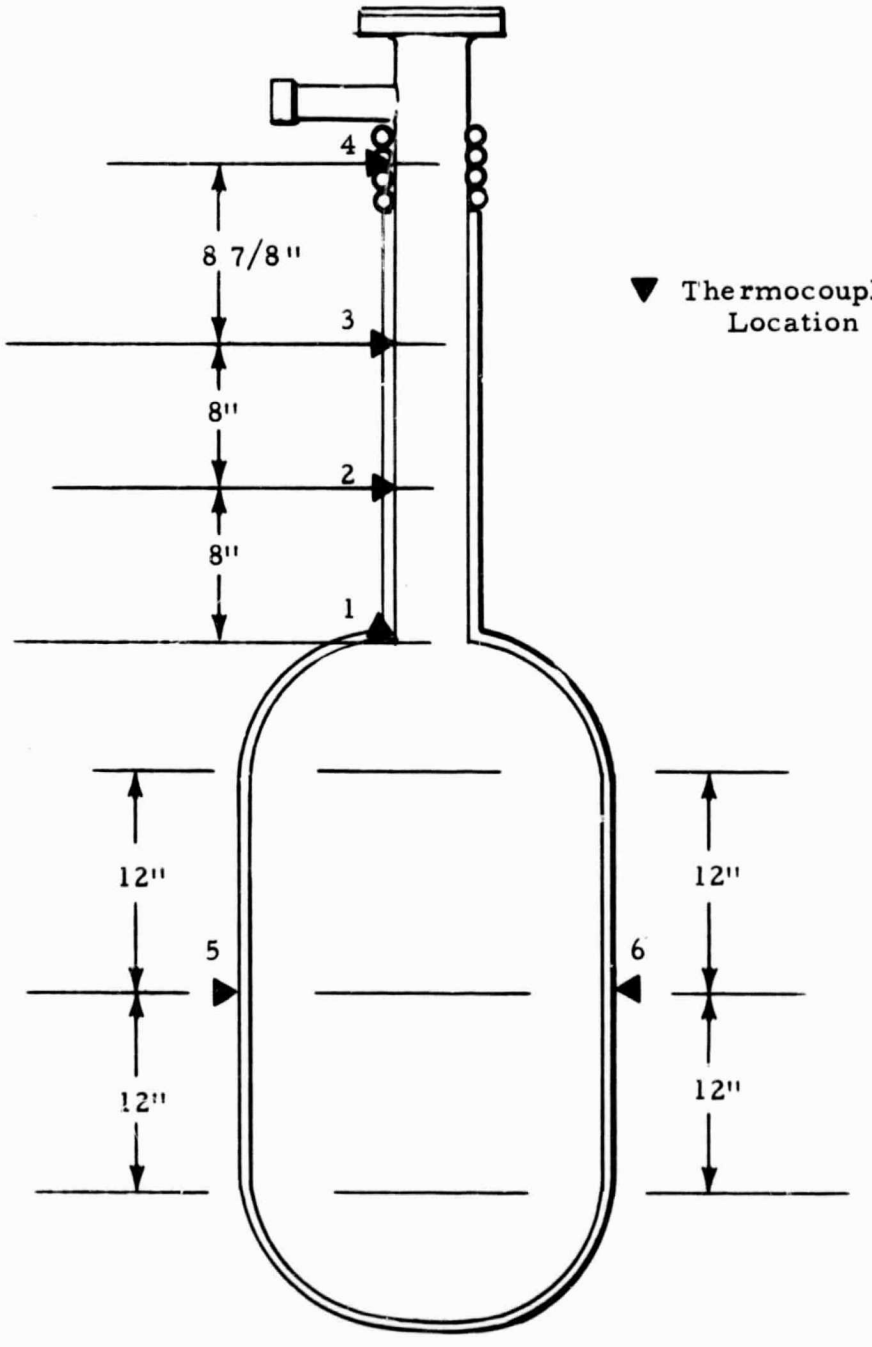

Fig. 27 - Lockheed/Huntsville-Installed Thermocouples

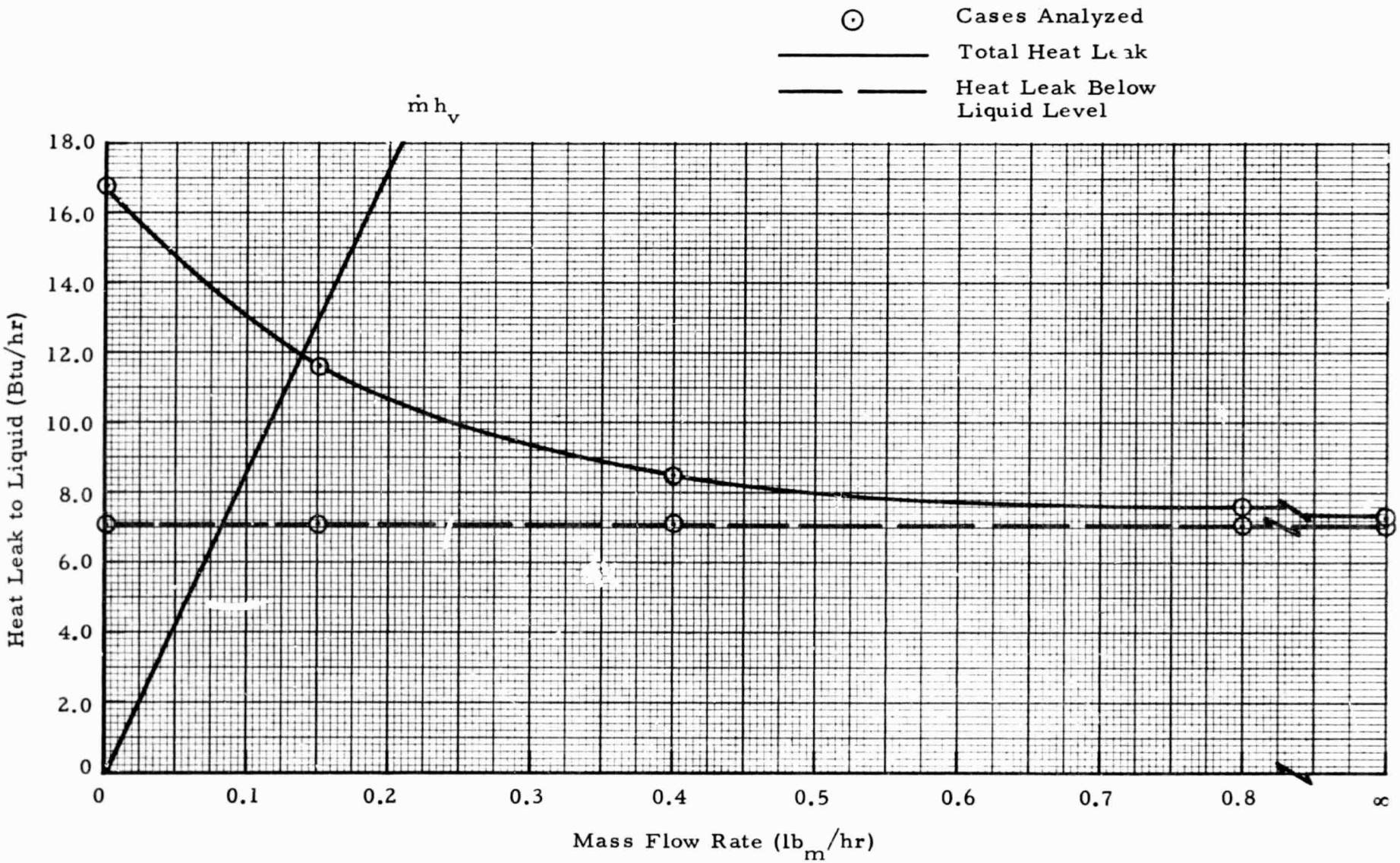

Fig. 28 - Heat Leak to Cryogen in 20-Inch Tank for Different Mass Flow Rates with Temperature-Dependent HPI Thermal Conductivity

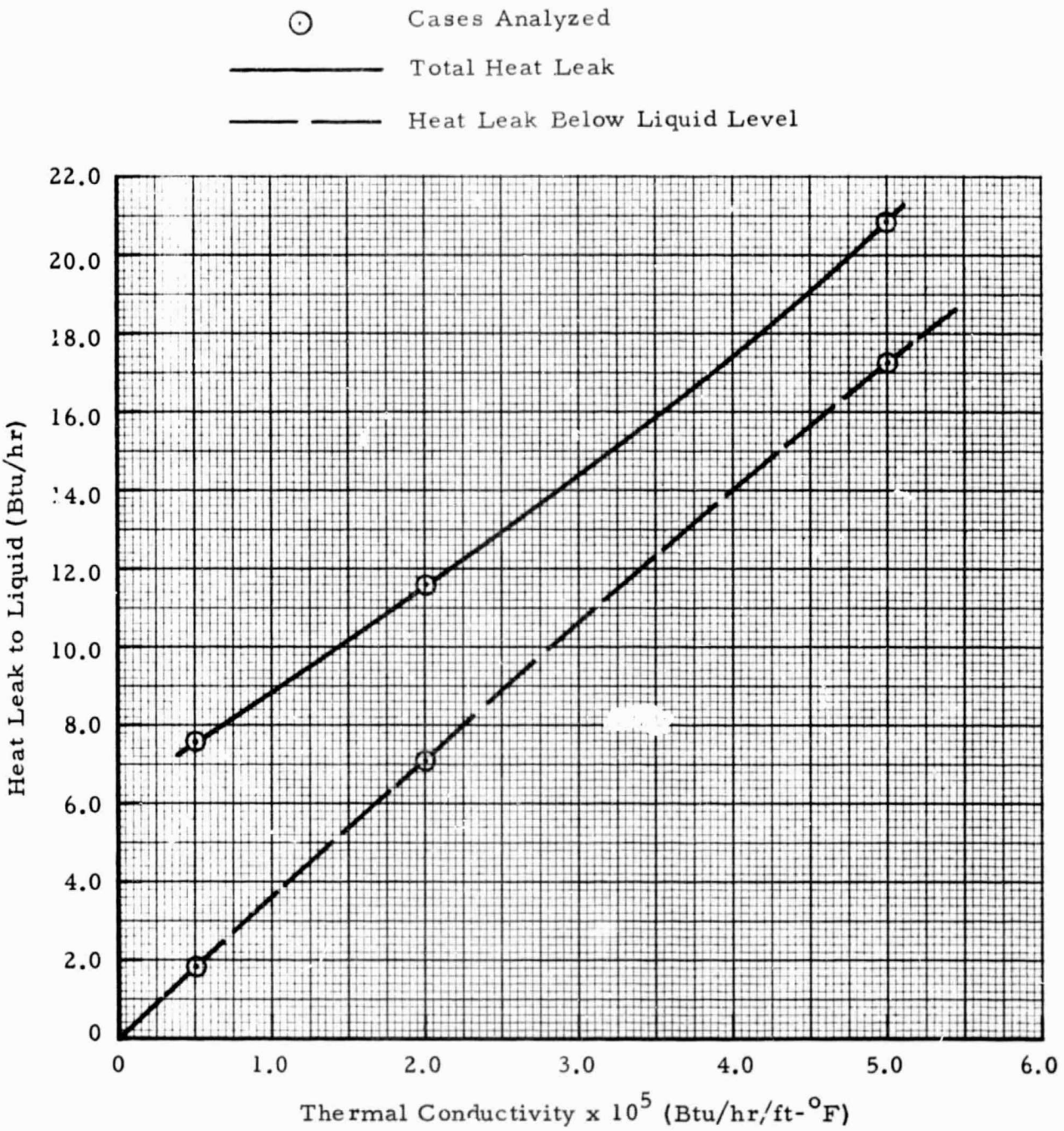

Fig. 29 - Heat Leak to Cryogen in 20-Inch Tank for Different HPI Conductivities with Equilibrium Vent Rates

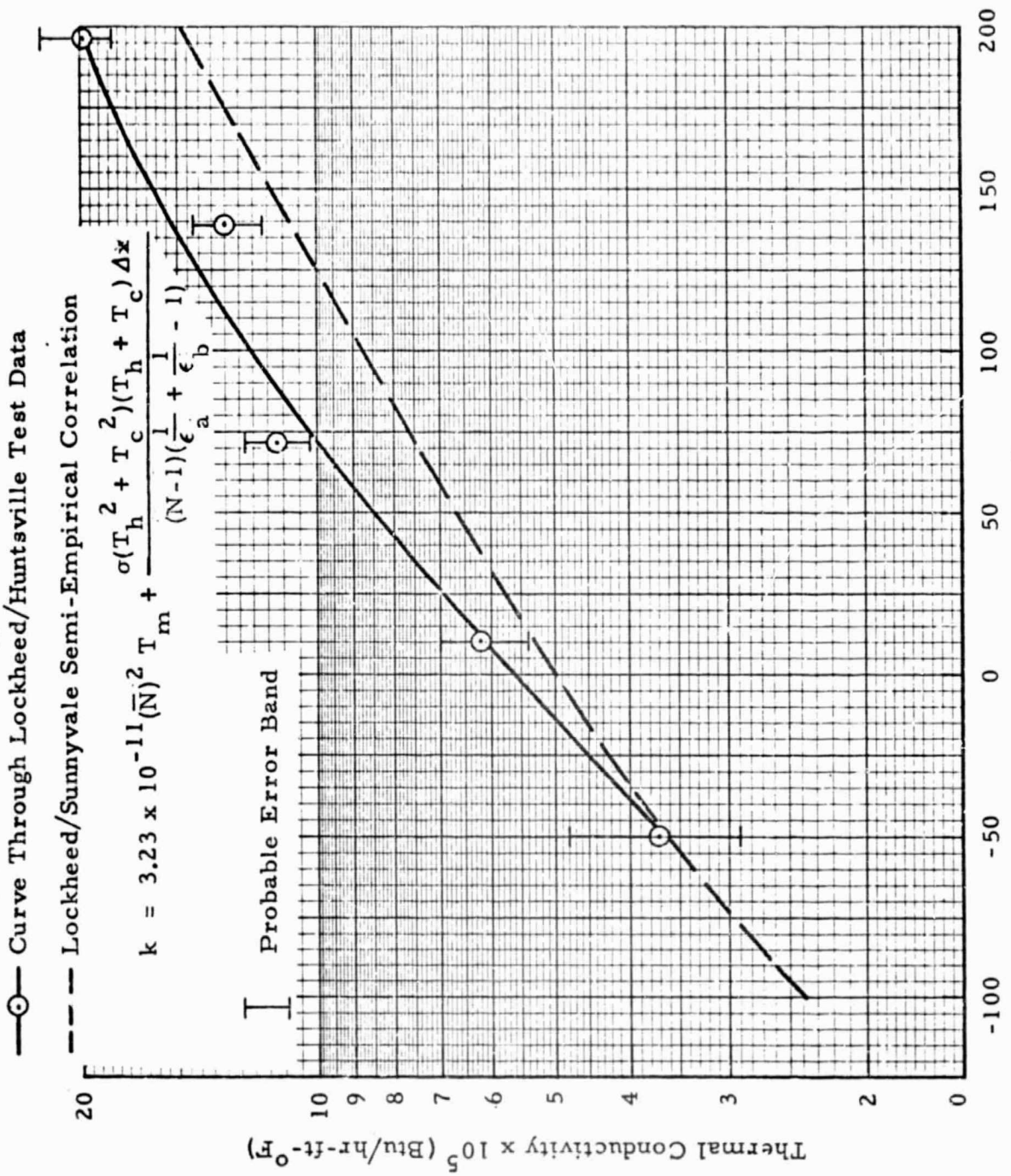

Fig. 30 - Temperature-Dependent Thermal Conductivity Data for 1/4-Mil Double Aluminized Mylar with Glass Fiber Needles (Superfloc) at 22 Layers per Inch

—⊙— Curve Through Lockheed/Huntsville Test Data

— — — Curve Through Lockheed/Sunnyvale Semi-Empirical Correlation

$$k = 5.9 \times 10^{-12} (\bar{N})^2 T_m + \frac{\sigma (T_h^2 + T_c^2) (T_h + T_c) \Delta x}{(N-1) \left(\frac{1}{\epsilon_a} + \frac{1}{\epsilon_b} - 1\right)}$$

— · — Curve Through Modified Lockheed/Sunnyvale Semi-Empirical Correlation

$$k = 5.9 \times 10^{-12} (\bar{N})^2 T_m + \frac{1.62\, \sigma (T_h^2 + T_c^2) (T_h + T_c) \Delta x}{(N-1) \left(\frac{1}{\epsilon_a} + \frac{1}{\epsilon_b} - 1\right)}$$

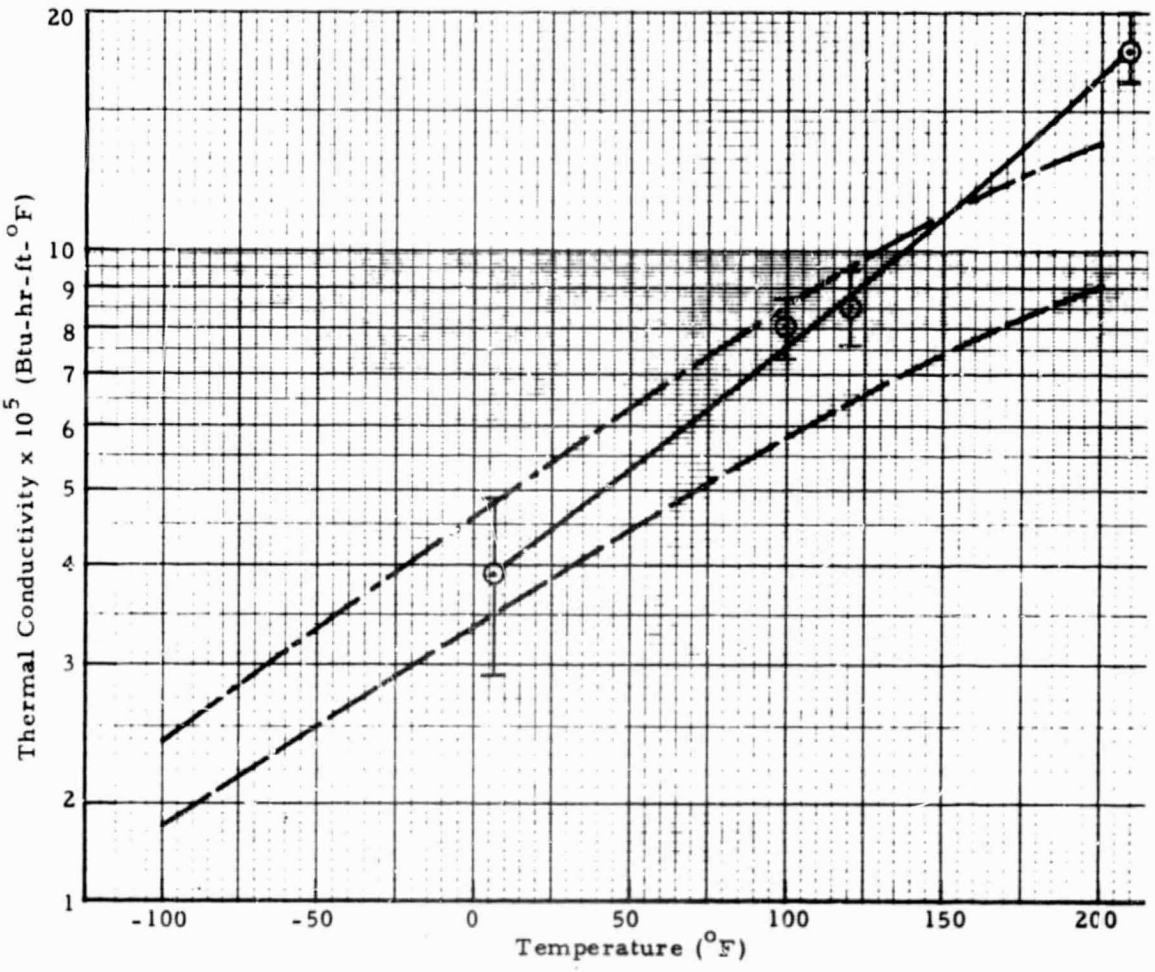

Fig. 31 - Temperature-Dependent Thermal Conductivity Data for 1/4-Mil Crinkled Perforated Singly Aluminized Mylar (NRC-2) at 70 Layers per Inch

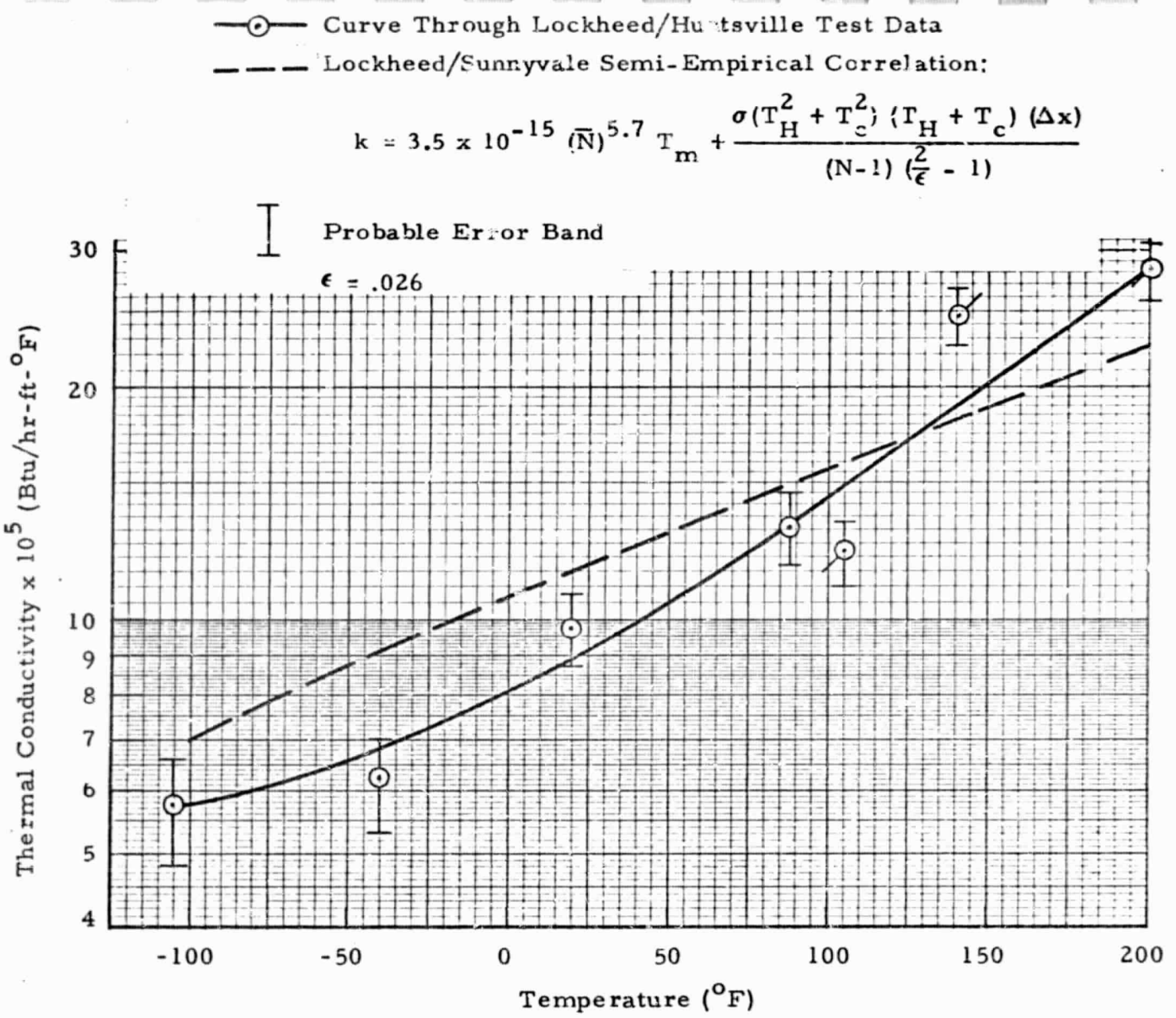

Fig. 32 - Temperature-Dependent Thermal Conductivity Data for 1/4-Mil Double Aluminized Mylar and Red Polyurethane Foam at 22 Layers per Inch

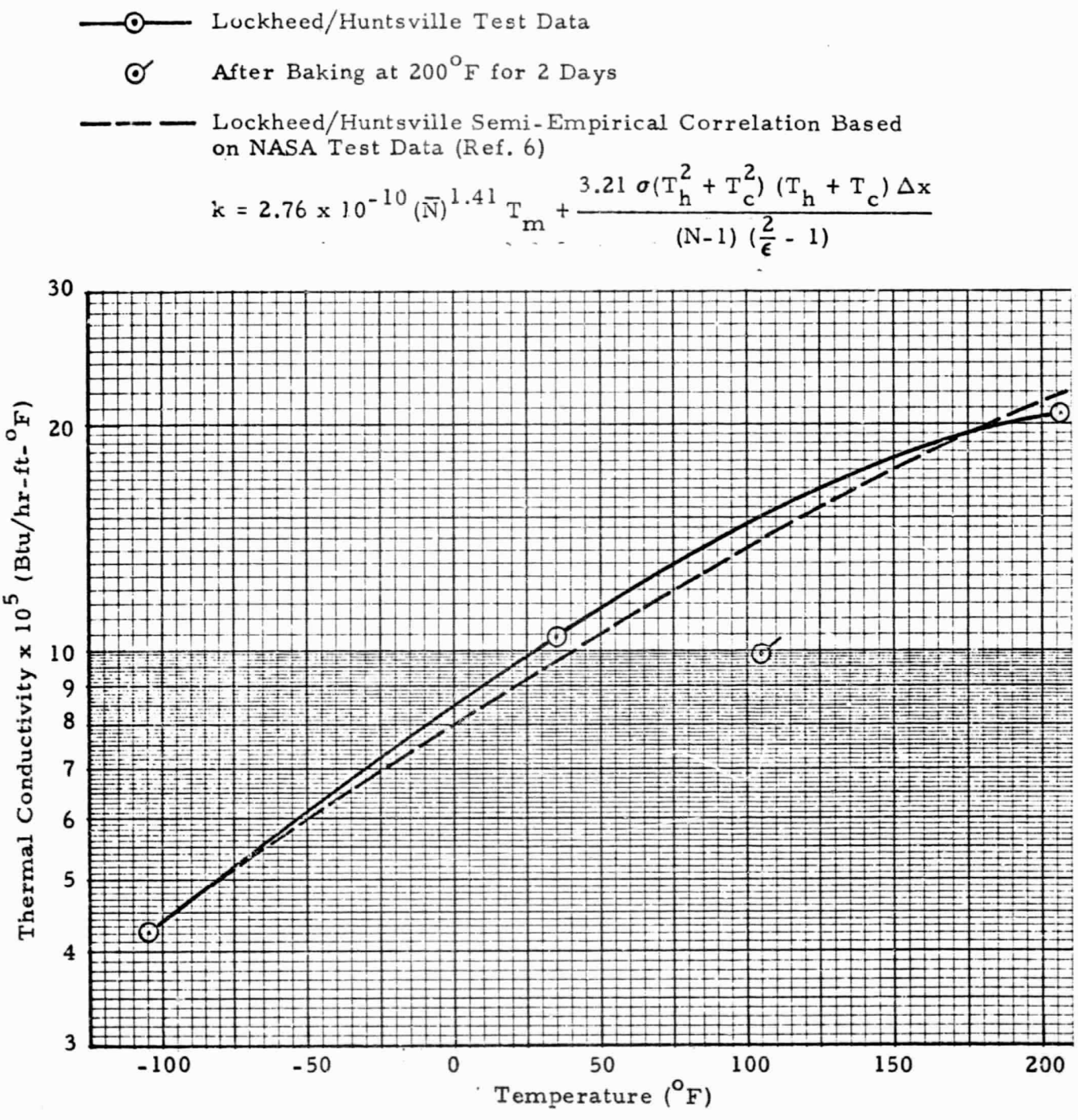

Fig. 33 - Temperature-Dependent Thermal Conductivity Data for 1/4-Mil Double Aluminized Mylar and Nylon Net at 50 Layers per Inch

Appendix A
KLINE-McCLINTOCK PROBABLE ERROR ANALYSIS PROCEDURE

If variables A and B have errors, a and b, respectively, then the propagation of these errors will be as follows:

For addition and subtraction of A and B, the resultant error P will be

$$P = \pm (a^2 + b^2)^{1/2}$$

For multiplication of A and B, the resultant error P will be

$$P = \pm \left[(Ab)^2 + (Ba)^2 \right]^{1/2}$$

For division of B by A, the resultant error P will be

$$P = \pm \left[\frac{\left(\frac{Ba}{A}\right)^2 + b^2}{A^2} \right]^{1/2}$$